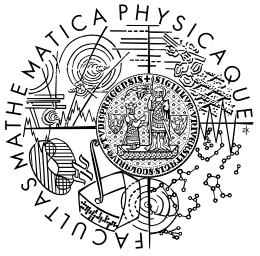

FACULTY
OF MATHEMATICS
AND PHYSICS
Charles University

BACHELOR THESIS

David Sychrovský

Comparison of Brill waves with the fields of singular rings

Institute of Theoretical Physics

Supervisor of the bachelor thesis:	doc. RNDr. Oldřich Semerák, DSc.
Study programme:	Physics
Study branch:	General Physics

Prague 2018

I declare that I carried out this bachelor thesis independently, and only with the cited sources, literature and other professional sources.

I understand that my work relates to the rights and obligations under the Act No. 121/2000 Sb., the Copyright Act, as amended, in particular the fact that the Charles University has the right to conclude a license agreement on the use of this work as a school work pursuant to Section 60 subsection 1 of the Copyright Act.

In ..... date ..... signature of the author

I would like to thank my supervisor doc. Oldřich Semerák for his patience and guidance throughout the work on this thesis and my friend Bc. Marek Liška for his help and useful advice on several occasions. I am grateful to my parents for supporting me during the studies. Last but not least I would like to thank my sister for truly untraditional motivation.

Title: Comparison of Brill waves with the fields of singular rings

Author: David Sychrovský

Department: Institute of Theoretical Physics

Supervisor: doc. RNDr. Oldřich Semerák, DSc., Institute of Theoretical Physics

Abstract:

Circular matter rings are a natural zero approximation of stationary and axially symmetric structures which appear in astrophysics. If the rings are infinitesimally thin (line sources), they are singular, which in the general relativistic description typically implies weird deformation of space in their vicinity. In particular, and contrary to the Newtonian picture, such rings even tend to behave in a strongly directional manner. One solution is to consider non-singular, extended sources (toroids), which may however be difficult to treat exactly and/or be unsatisfactory in other respects. In this thesis we check another option, namely to abandon the "real matter" completely and consider a non-singular source represented by mere curvature arranged, at least at some instant, in a pattern possessing the above symmetries. One such solution of Einstein's equations is known as the Brill waves; we study its properties at the moment of time symmetry (when it is momentarily static), in order to compare it with the space-times of matter rings.

Keywords:

thin axially symmetric rings, Brill waves in the moment of time symmetry, static Brill wave approximation.

Contents

Introduction

Black holes are one of the most notable predictions of general relativity. Despite primary skepticism about their physical significance, these objects nowadays play a key role in a standard picture of several types of astrophysical systems, namely galactic nuclei (including that of our Galaxy), high-mass X-ray binaries and gamma-ray bursts. Besides a broad evidence inferred from effects caused by interaction of putative black holes with matter, radiation and fields in accretion systems, a further support for their existence has recently been provided by direct detections of gravitational waves. Actually, although it was an inspiral and merger of a neutron-star binary that was expected as the most probable source of sufficiently strong waves, four of the five events announced so far rather fit numerical templates generated by black-hole binaries of relatively large masses.

As a result of gravitational attraction and centrifugal repulsion, a typical configuration of matter inflowing, in a quasi-stationary manner and with a non-zero angular momentum, to a compact center has the geometry of a disc, a ring or a toroid. In accretion models, gravity of this "outer" matter is usually neglected, although it may in fact dominate higher derivatives of the field (curvature). Wishing to model the accretion-system field exactly, one naturally approximates the accretion matter by some stationary (or even static) and axially symmetric solution of the Einstein equations whose source (support of the energy- momentum tensor) is of some of the above shapes. Due to the non-linearity of Einstein's equations, it is generally very difficult to "superpose" their solutions, but in some simple cases, like in the static and axially symmetric one, it is at least partially possible. In particular, a vacuum space-time of such symmetries can be described by the so-called Weyl metric

$$\mathrm{d}s^2 = -N^2\mathrm{d}t^2 + N^{-2}\left[\rho^2\mathrm{d}\phi^2 + e^{2\lambda}(\mathrm{d}\rho^2 + \mathrm{d}z^2)\right], \tag{1}$$

where the lapse N is often being expressed as $N \equiv e^{\nu}$ in terms of a gravitational potential ν which satisfies the Laplace equation (and thus superposes linearly like in the Newtonian theory). The second metric function λ is determined by line integral of an expression given by gradient of ν; it is zero on the symmetry axis $\rho = 0$ (at least if no source is there). The time t and azimuth ϕ are adapted to the Killing symmetries, the other two coordinates covering the meridional plane (perpendicular to both the existing symmetries), ρ standing for the cylindrical radius and z being the "vertical" coordinate. Due to axial symmetry both metric functions ν and λ only depend on ρ and z.

In such a way, within the static and axisymmetric class of space-times, the description of the black hole surrounded by an accretion disc, ring or toroid starts from summing the potential ν corresponding to a Schwarzschild black hole with that due to some of the above configurations. On the level of potential, the exercise thus reduces to its Newtonian version. However, in relativity, the second metric function λ is important as well: it affects the geometry of the meridional plane, so it can strongly modify the original "Newtonian" picture. The difference between the Newtonian and relativistic pictures is most pronounced for what is a straightforward counter-part of an ordinary Newtonian ring (infinitesimally thin circle) – the so-called Bach-Weyl ring. Actually, in that case λ deforms space to such an extent that the ring ceases to be locally cylindrical, even lying at infinite proper distance when approached from its "inside" (from the region of lower radii ρ).

Other ring sources have been proposed as physically more acceptable, most notably the one obtained within the Majumdar-Papapetrou class of solutions [1] which have $\lambda = 0$. This ring is locally cylindrical and its geometric measures behave much more naturally, but physically it corresponds to an extremally charged matter, which also does not seem to be astrophysically realistic. In addition, even such a "more reasonable" ring is anyway infinitesimally thin, and thus singular (curvature diverges at its location). This can of course be overcome by considering a toroid (of non-zero cross section) instead of a spatially one-dimensional ring.

Another option (which we will check in this thesis) is to consider a vacuum space-time where however curvature peaks on a circle. Such a situation can be expected to be non-stationary, but one could take its "snapshot" at the moment of time symmetry (provided that such a moment at all exists). Actually, there exists a solution of Einstein's equations which does have such properties: it is called Brill waves and corresponds to an axially symmetric configuration of gravitational waves which converge to a ring-like pattern (curvature gets maximal on a circle) and then disperse again in a time-symmetric way. In this thesis, we wish to compute basic geometrical parameters of Brill-wave space at the moment of time symmetry and compare them with those characterizing the above mentioned ring sources, in order to learn whether the momentarily static Brill solution could be employed as a non-singular approximation of a ring source in general relativity.

The thesis is organized as follows. In Chapter 1, we outline basic features of the Brill solution in the moment of time-symmetry. In Chapter 2, the thin-ring sources are described. In Chapter 3, we compute several geometric invariants known about the thin-rings. Chapter 4 introduces some basic methods of the evolution of Brill waves. In Chapter 5, we outline the consequences of considering the Brill solution static. Chapter 6 covers the second, less commonly used form of the seed function, which characterizes the Brill space. Finally, in Chapter 7, we focus on the motion of photons and test particles in the static Brill space-time. We employ geometrized units i.e. $c = G = 1$ and Einstein's summation rule[1]. Indexes after a comma stand for a partial derivative with respect to that variable.

[1]The pair Latin indexes represent the summation over the 3-space coordinates, while the Greek indexes indicate summation over all 4 dimensions of the space-time. Symbols used for coordinates stand for the individual components of a given tensor.

1. Characteristics of the Brill solution

The Brill waves are a axially symmetric vacuum solution of Einstein's equations whose 3-metric γ_{ii}[1] in cylindrical coordinates (z, ρ, ϕ) at the moment of time symmetry is given by [2]

$$\mathrm{d}\tilde{l}^2 = e^{2q(\tilde{\rho},\tilde{z})}(\mathrm{d}\tilde{\rho}^2 + \mathrm{d}\tilde{z}^2) + \tilde{\rho}^2\mathrm{d}\phi^2, \tag{1.1}$$

where $q = q(\tilde{\rho}, \tilde{z})$ is the seed function which on a regular axis of symmetry has to satisfy $q(\tilde{z}, 0) = q_{,\tilde{\rho}}(\tilde{z}, 0) = 0$, and which is usually chosen as[2]

$$q(\tilde{\rho}, \tilde{z}) = A\left(\frac{\tilde{\rho}}{\sigma}\right)^2 e^{-\frac{(\tilde{\rho}-\tilde{\rho}_0)^2+(\tilde{z}-\tilde{z}_0)^2}{\sigma^2}}, \tag{1.2}$$

where A is a dimensionless measure of amplitude of the wave, and σ is its wavelength. In this thesis we set $\tilde{z}_0 = 0\ m$ thereby fixing the coordinate center in the "vertical" direction. We then define the new dimensionless variables according to

$$\begin{aligned} \rho &= \frac{\tilde{\rho}}{\sigma}, \\ \rho_0 &= \frac{\tilde{\rho}_0}{\sigma}, \\ z &= \frac{\tilde{z}}{\sigma}. \end{aligned} \tag{1.3}$$

Equations (1.1) and (1.2) then become

$$\begin{aligned} \mathrm{d}l^2 &= e^{2q(\rho,z)}(\mathrm{d}\rho^2 + \mathrm{d}z^2) + \rho^2\mathrm{d}\phi^2, \\ q(\rho, z) &= A\rho^2 e^{-(\rho-\rho_0)^2-z^2}, \end{aligned} \tag{1.4}$$

where we have defined the dimensionless line element $l \overset{\text{def.}}{=} \frac{\tilde{l}}{\sigma}$.

Mainly for the purposes of time evolution, the metric is conformally transformed $\gamma_{ii} = \psi^4\overline{\gamma}_{ii}$ such that it has vanishing scalar curvature, $\overline{R}^i{}_i = 0$. The momentum constraint is then satisfied trivially and the Hamiltonian constraint becomes [2]

$$4[\nabla^2 \ln(\psi) + |\boldsymbol{\nabla} \ln(\psi)|^2] + \nabla^2 q - \frac{q_{,\rho}}{\rho} = 0, \tag{1.5}$$

where $\boldsymbol{\nabla}$ denotes the flat-space 3-gradient $\boldsymbol{\nabla} = \left(\frac{\partial}{\partial x}, \frac{\partial}{\partial y}, \frac{\partial}{\partial z}\right)$ and ψ is the conformal factor. We also assume that ψ goes to the Schwarzschild form at radial infinity

$$\psi = 1 + \frac{m}{2r} + o\left(\frac{1}{r^2}\right), \quad as\ r \to \infty, \tag{1.6}$$

where m denotes the total mass-energy content of the Brill wave space-time and r is the sperical radius which, at least asymptotically, relates to the Weyl coordinates as $r = \sqrt{\rho^2 + z^2}$. It can also be shown that the seed function $q(\rho, z)$ falls of as $\sim \frac{1}{r^2}$ as $r \to \infty$ [2].

[1] We choose to denote γ_{ij} the Brill 3-metric in the moment of time symmetry, $\overline{\gamma}_{ij}$ its conformal transformation (see Chapter 4) and $g_{\mu\nu}$ the 4-dimensional metric given in Chapter 5.

[2] See Section 6 for another suitable form of the seed function.

We will set the imaginary "ring" in the Brill space-time where the radial part of the metric reaches its maximum, i.e., where

$$0 = \frac{\partial e^{q(\rho,0)}}{\partial \rho} = 2A\rho[1 - \rho(\rho - \rho_0)]e^{-(\rho-\rho_0)^2} e^{q(\rho,0)},$$

which has only one interesting solution (since the axial and reflection symmetry about the equatorial plane requires $q_{,\rho}(0, z) = 0$)

$$\rho_{\max} = \frac{\rho_0 + \sqrt{\rho_0^2 + 4}}{2} \in (0, \infty). \tag{1.7}$$

To visualize the motivation behind this thesis Figure 1.1 shows the radial part of the metric (1.1) in the moment of time symmetry in the $z = 0$ and $z = 1$ plane with $A = 1, \rho_0 = 1$. Although the maximum of the metric has no invariant meaning, we will see in Chapters 4 and 5 that it approaches an extreme of the Ricci scalar along the ρ-axis in the limit of high negative/positive values of ρ_0 for positive/negative values of the amplitude A.

We will also occasionally transform the metric (1.1) to toroidal coordinates (ζ, ϕ, ψ), $\zeta \in [0, \infty)$, $\psi \in [0, 2\pi)$ which are given by

$$\begin{aligned} \rho &= \rho_{\max} \frac{\sinh \zeta}{\cosh \zeta - \cos \psi}, \\ z &= \rho_{\max} \frac{\sin \psi}{\cosh \zeta - \cos \psi}, \\ \phi &= \phi, \end{aligned} \tag{1.8}$$

which gives

$$\begin{aligned} \mathrm{d}l^2 &= \rho_{\max}^2 \frac{e^{2q}(\mathrm{d}\zeta^2 + \mathrm{d}\psi^2) + \sinh^2 \zeta \, \mathrm{d}\phi^2}{(\cosh \zeta - \cos \psi)^2}, \\ q(\zeta, \psi) &= A\rho_{\max}^2 \frac{\sinh^2 \zeta}{(\cosh \zeta - \cos \psi)^2} \exp\left(- \frac{(\rho_{\max} \sinh \zeta - \rho_0)^2 + \rho_{\max}^2 \sin^2 \psi}{(\cosh \zeta - \cos \psi)^2} \right). \end{aligned} \tag{1.9}$$

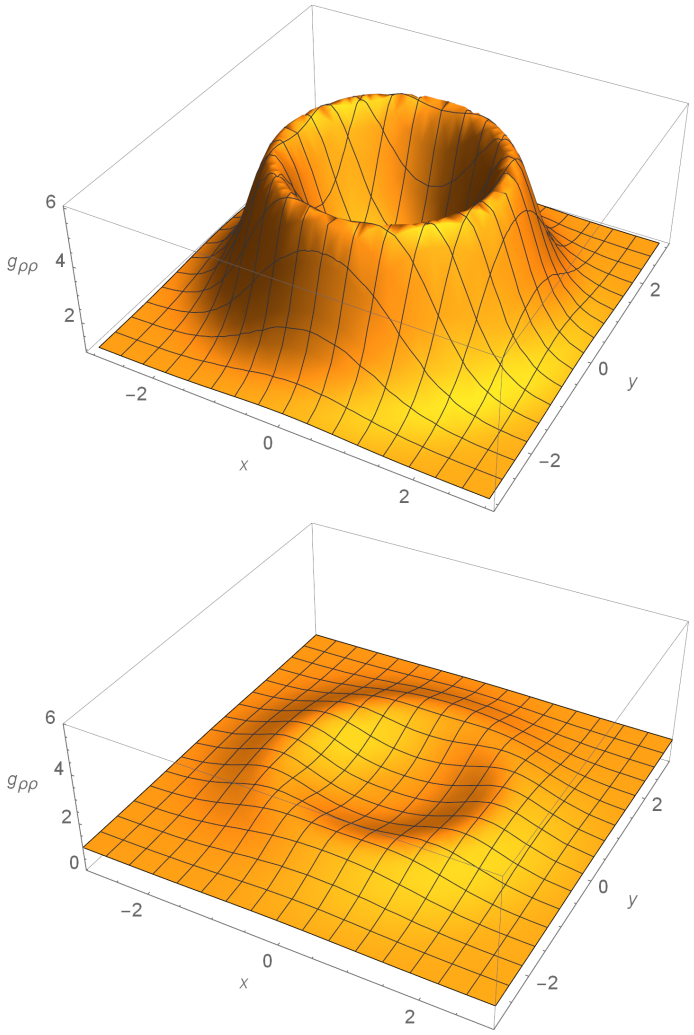

Figure 1.1: The radial part of the Brill metric (1.1) for $\rho_0 = 1$ at $z = 0$ (top) and $z = 1$ (bottom).

2. Ring sources

In the static axisymmetric vacuum case, the Einstein equations can in the Weyl coordinates be reduced to the Laplace equation for the gravitational potential ν and two equations for the two components of gradient of the second metric function λ (determined by the gradient of ν). Despite the uniqueness of the Laplace-equation solutions, one can consider different boundary conditions and thus different solutions even for a similar type of source.

Focusing on the circular ring sources, one can — for instance — consider the Bach-Weyl (B-W) ring, the Majumdar-Papapetrou (M-P) ring and the Appell ring(s). The Bach-Weyl ring is the general-relativity counter-part of the "ordinary" Newtonian homogeneous circular thin ring. In spite of (therefore) being also employed as the simplest ring source in GR, the geometry is strongly deformed (directional) in its vicinity due to the function λ which has no Newtonian analog. The Majumdar-Papapetrou—type ring is extremally charged and corresponds to $\lambda = 0$, hence it generates much more satisfactory geometry (in particular, it is *not* directional, i.e. it is locally cylindrical). The Appell rings (and specifically their simplest case) have non-trivial, double-sheeted topology similar to the Kerr solution, namely their non-singular interior interconnects two distinct asymptotically flat regions, effectively "switched over" by changing the sign of the ring-mass parameter.

We refer the reader to paper [1] for details on these ring sources (and their comparison with the *stationary* Kerr ring source), only reproducing here Table 2.1 where basic geometric parameters of the above rings are summarized.

Ring	Small circumference	Large circumference	Proper distance to/radius	Proper enclosed area	$\rho_{\max} \to 0^+$ limit
M-P	Zero	Infinite	Finite from all directions	Finite	Extreme R-N horizon
B-W	Infinite (on $\rho < \rho_{\max}$ side)	Infinite	Finite/infinite from $\rho \geq \rho_{\max}/\rho < \rho_{\max}$ ($\implies$ infinite proper radius)	Infinite	Curzon singularity
Appell	Infinite (on $\cos(2\psi) < 0$ side)	Finite from $\psi = \pi$ side, Infinite from elsewhere	Finite/infinite from $\cos(2\psi) \geq 0/ < 0$, ($\implies$ infinite proper radius)	Finite	Curzon singularity
Kerr	Zero	Finite from $r = 0$ side, Infinite from elsewhere	Finite from all directions	Finite	Schwarzs-child singularity

Table 2.1: Basic features of the ring sources compared with the Brill-wave solution in this thesis. R-N stands for Reissner-Nordström. Individual coordinates and parameters have been defined in Chapter 1.

3. Geometrical invariants of the "ring"

We will now compute several important invariants known for the different thin-ring sources and compare them with those found for the Brill metric (1.1).

3.1 Small circumference

The "small circumference" l is defined as the circumference of the circle in the meridional $(z-\rho)$ plane centered at $z=0$, $\rho=\rho_{\max}$ whose radius goes to zero. For some of the thin-ring sources this quantity does not vanish due to extreme behavior of the metric in close proximity of the ring and it may also depend on the direction in which the ring is approached [1], see Table 2.1. We choose to calculate the small circumference in toroidal coordinates

$$l=\lim_{k\to\infty}\oint\sqrt{g_{\psi\psi}(k,\psi)}\,\mathrm{d}\psi=\lim_{k\to\infty}\int_0^{2\pi}\rho_{\max}\frac{e^{q(k,\psi)}}{\cosh k-\cos\psi}\,\mathrm{d}\psi. \tag{3.1}$$

The integrand behaves as $\sim e^{Ae^{1+e^{-2k}}}e^{-k}$ in the limit $k\to\infty$. We can thus find an integrable function

$$G(k,\psi)=Ce^{\tilde{A}e^2},$$

such that $G(k,\psi)\geq|\sqrt{g_{\psi\psi}(k,\phi,\psi)}|$ and therefore we can use the continuous dependence of an integral on a parameter theorem to get

$$l=0,$$

which is what one would expect from a "well-behaved" metric.

3.2 Large circumference

The "large circumference" L is defined as the circumference of a circle centered at the origin with the "coordinate" radius $\rho_{\max}$. It can be calculated by

$$L=\lim_{k\to\infty}\oint\sqrt{g_{\phi\phi}(k,\psi)}\,\mathrm{d}\phi=\lim_{k\to\infty}2\pi\sqrt{g_{\phi\phi}(k,\psi)}=\lim_{k\to\infty}\frac{2\pi\rho_{\max}\sinh k}{\cosh k-\cos\psi}=2\pi\rho_{\max}. \tag{3.2}$$

We note that L does not depend on the choice of the seed function and thus any circle of finite radius centered at the origin in the Brill space-time has a finite circumference since $\rho_{\max}$ can for the purpose of defining toroidal coordinates be chosen arbitrarily.

3.3 Proper radius and distance

The proper radius of the ring in cylindrical coordinates is given by

$$b = \int_0^{\rho_{\max}} \sqrt{g_{\rho\rho}(\rho, 0)}\, \mathrm{d}\rho = \int_0^{\rho_{\max}} e^{A\rho^2 e^{-(\rho-\rho_0)^2}}\, \mathrm{d}\rho. \tag{3.3}$$

Note that the integrand is continuous and finite for all $\rho \in \mathbb{R}$, and thus the integral is finite for all finite radii $\rho_{\max}$. The proper radius b is also monotonically increasing function of A and ρ_0 for positive values of the amplitude A. We will show that by taking the following derivatives

$$\frac{\partial b}{\partial A} = \frac{\partial}{\partial A} \int_0^{\rho_{\max}} \exp\Big[A\rho^2 e^{-(\rho-\rho_0)^2}\Big]\, \mathrm{d}\rho = \int_0^{\rho_{\max}} \rho^2 e^{-(\rho-\rho_0)^2} \exp\Big[A\rho^2 e^{-(\rho-\rho_0)^2}\Big]\, \mathrm{d}\rho > 0,$$

where we have used the fact that the integral is finite to swap differentiation and integration. The inequality follows from the fact that the integrand is positive $\forall A \in \mathbb{R}$ and $\forall \rho_0 \in \mathbb{R}$.

Similarly we get

$$\frac{\partial b}{\partial \rho_0} = \frac{\partial}{\partial \rho_0} \int_0^{\rho_{\max}} e^{A\rho^2 e^{-(\rho-\rho_0)^2}}\, \mathrm{d}\rho = \int_0^{\rho_{\max}} \frac{\partial}{\partial \rho_0}(e^{A\rho^2 e^{-(\rho-\rho_0)^2}})\, \mathrm{d}\rho + e^{A\rho_{\max}^2 e^{-(\rho_{\max}-\rho_0)^2}} \frac{\partial \rho_{\max}}{\partial \rho_0} =$$
$$2A \int_0^{\rho_{\max}} (\rho-\rho_0)\rho^2 \exp\Big[A\rho^2 e^{-(\rho-\rho_0)^2} - (\rho-\rho_0)^2\Big]\, \mathrm{d}\rho + e^{A\rho_{\max}^2 e^{-(\rho_{\max}-\rho_0)^2}} \Big(\frac{1}{2} + \frac{\rho_0}{2\sqrt{\rho_0^2+4}}\Big).$$

The second term is positive, bounded in $(0, 1)$. The first term for $A > 0$ is positive if

$$0 < \int_0^{\rho_{\max}} (\rho-\rho_0)\rho^2 e^{A\rho^2 e^{-(\rho-\rho_0)^2} - (\rho-\rho_0)^2}\, \mathrm{d}\rho \Leftrightarrow$$
$$\int_0^{\rho_0} (\rho_0-\rho)\rho^2 e^{A\rho^2 e^{-(\rho-\rho_0)^2} - (\rho-\rho_0)^2}\, \mathrm{d}\rho < \int_{\rho_0}^{\rho_{\max}} (\rho-\rho_0)\rho^2 e^{A\rho^2 e^{-(\rho-\rho_0)^2} - (\rho-\rho_0)^2}\, \mathrm{d}\rho \Leftrightarrow$$
$$1 > \frac{\int_{\rho_0}^{\rho_{\max}} (\rho-\rho_0)\rho^2 \exp\Big[A\rho^2 e^{-(\rho-\rho_0)^2} - (\rho-\rho_0)^2\Big]\, \mathrm{d}\rho}{\int_0^{\rho_0} (\rho_0-\rho)\rho^2 \exp[A\rho^2 e^{-(\rho-\rho_0)^2} - (\rho-\rho_0)^2]\, \mathrm{d}\rho} \overset{\text{def.}}{=} \Sigma, \tag{3.4}$$

where both integrands (and thus the integrals) are positive for $\rho_0 \in \mathbb{R}^+$. To shows the behavior of $\Sigma = \Sigma(\frac{1}{\rho_0})$ and $\Sigma = \Sigma(\rho_0)$ near the origin i.e. as $\rho_0 \to \infty$ and as $\rho_0 \to 0^+$ respectively we plot the functions in Figure 3.1. It shows that the inequality (3.4) holds $\forall \rho_0 \in \mathbb{R}^+$. For $\rho_0 \in \mathbb{R}^-$ the integrand is positive and thus b is a monotonically increasing function of $A > 0$ and $\rho_0 \in \mathbb{R}$. For negative values of the amplitude inequality (3.4) does not hold $\forall \rho_0 \in \mathbb{R}$. Figure 3.2 shows the derivative of the proper radius as a funcion of ρ_0 and A in the region of negative amplitudes. The derivative is possitive at certain points. However, for example for $A = -4$ and $\rho_0 = 0$ we get

$$\frac{\partial b}{\partial \rho_0} \doteq -0.213,$$

and thus the proper radius can decrease with the "coordinate" radius $\rho_{\max}$ for negative values of the amplitude A.

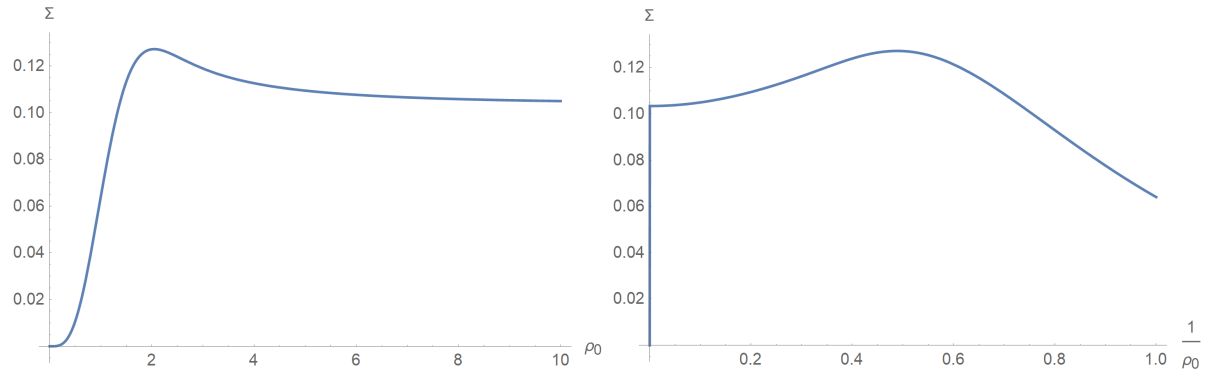

Figure 3.1: Σ (see Eq. 3.4) as a function of the measure of radius ρ_0 and its inverse.

For given values of the parameters A and ρ_0 the integral (3.3) can be solved numerically. For example for $A = 1$ and $\rho_0 = 1$ we get

$$b \doteq 4.28.$$

To further illustrate the behavior of the proper radius for positive amplitudes, we plot (3.3) in Figure 3.3 as a function of the measure of radius $\rho_0 \in (0, 1)$ and amplitude $A \in (0, 1)$.

We next focus on finding the proper distance d to the "ring" from a arbitrary point in the same meridional plane. In toroidal coordinates $(\tilde{\zeta}, \tilde{\phi}, \tilde{\psi})$ the proper distance d takes a simple form

$$d = \int_{\tilde{\zeta}}^{\infty} \sqrt{g_{\zeta\zeta}(\zeta, \tilde{\psi})}\, \mathrm{d}\zeta = \int_{\tilde{\zeta}}^{\infty} \frac{\rho_{\max} e^{q(\zeta,\tilde{\psi})}}{\cosh\zeta - \cos\tilde{\psi}}\, \mathrm{d}\zeta. \tag{3.5}$$

The integrand behaves as $\sim e^{-\zeta}$ for $\zeta \to \infty$ and is continuous, so the proper distance d is finite from all points in the meridional plane.

Alternatively, one can perform the calculation in cylindrical coordinates. We are interested in the proper distance from $(0, 0, \rho_{\max}, \phi)$ to an arbitrary point $(0, \tilde{z}, \tilde{\rho}, \phi)$ in the same meridional plane (same ϕ). The line $\mathcal{L}$ connecting the two points in parametric representation is

$$\begin{aligned} \rho &= k\ \cos\alpha + \rho_{\max}, \\ z &= k\ \sin\alpha, \end{aligned} \tag{3.6}$$

where $k \in [0, \frac{\tilde{z}}{\sin\alpha}]$ is the line parameter and $\alpha = \arctan\left(\frac{\tilde{z}}{\tilde{\rho}}\right)$ is the angle between the ρ-axis and the line (3.6). The line element is given by

$$\mathrm{d}\iota = \sqrt{g_{\mu\nu} n^\mu n^\nu}\, \mathrm{d}k,$$

where

$$n^\mu = \frac{1}{\sqrt{1 + \tan^2(\alpha)}} (0, \tan(\alpha), 1, 0)$$

is the tangent vector to the line of unit length. Therefore the proper distance in cylindrical coordinates is given by

$$d = \left|\int_{\mathcal{L}} \mathrm{d}\iota\right| = \left|\int_0^{\frac{\tilde{z}}{sin\alpha}} \sqrt{g_{\mu\nu}n^\mu n^\nu}\ \mathrm{d}k\right| =$$

$$\left|\int_0^{\frac{\tilde{z}}{sin\alpha}} \sqrt{g_{\rho\rho}(k\ \sin\alpha, k\ \cos\alpha + \rho_{\max})}\sqrt{\left(\frac{\partial\rho}{\partial k}\right)^2 + \left(\frac{\partial z}{\partial k}\right)^2}\ \mathrm{d}k\right| =$$

$$\left|\int_0^{\frac{\tilde{z}}{\sin\alpha}} \exp\Big[A(k\cos\alpha + \rho_{\max})^2 e^{-(k\cos\alpha+\rho_{\max}-\rho_0)^2-k^2\sin^2\alpha}\Big]\sqrt{\cos^2\alpha + \sin^2\alpha}\ \mathrm{d}k\right| =$$

$$\left|\int_0^{\frac{\tilde{z}}{\sin\alpha}} \exp\Big[A(k\cos\alpha + \rho_{\max})^2 e^{-(k\cos\alpha+\rho_{\max}-\rho_0)^2-k^2\sin^2\alpha}\Big]\ \mathrm{d}k\right| \quad (3.7)$$

Figure 3.4 shows a contour plot of the proper distance to the "ring" d for $A = 1$, $\rho_0 = 0$ and $\rho_0 = 1$.

3.4 Proper area of the "ring"

The area S is given in cylindrical coordinates as

$$S = \int_0^{2\pi}\int_0^{\rho_{\max}} \sqrt{g_{\rho\rho}(\rho,0)g_{\phi\phi}(\rho,0)}\ \mathrm{d}\rho\mathrm{d}\phi = 2\pi\int_0^{\rho_{\max}} \rho\exp\Big[A\rho^2 e^{-(\rho-\rho_0)^2}\Big]\ \mathrm{d}\rho. \quad (3.8)$$

This integral cannot be expressed in terms of standard mathematical functions, but it can be evaluated numerically. For example, for $A = 1$ and $\rho_0 = 1$ we get

$$S \doteq 29.47.$$

This differs from the Euclidean relation

$$\tilde{S} \equiv \pi b^2 \doteq 57.55,$$

where b denotes the proper radius of the "ring". This difference demonstrates the curvature of space. Figure 3.5 shows the proper area S and the Euclidean area $\tilde{S}$ as a function of ρ_0. Due to the curvature of space the Euclidean area grows faster. Both approach zero for $\rho_0 \to -\infty$ since $\rho_{\max} \overset{\rho_0\to-\infty}{\to} 0^+$ and thus even $r \overset{\rho_0\to-\infty}{\to} 0^+$. We will focus on this limit in the next Section.

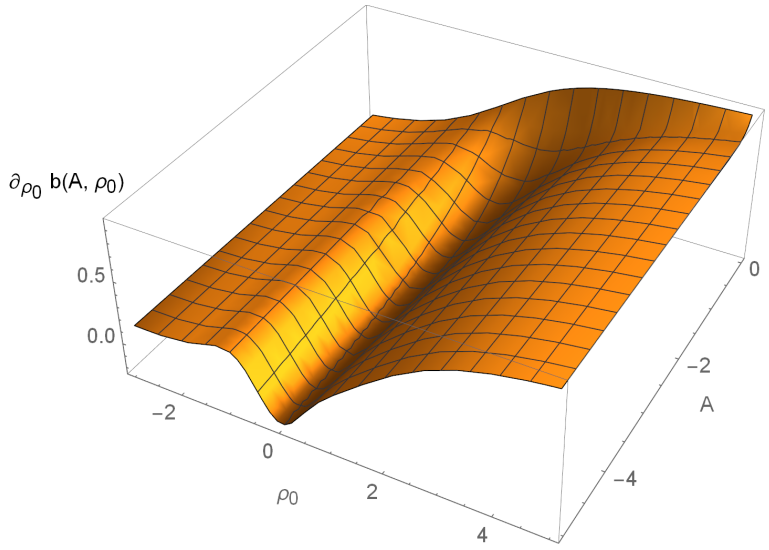

Figure 3.2: The derivative of the proper radius as a funcion of ρ_0 and A in the region of negative amplitudes.

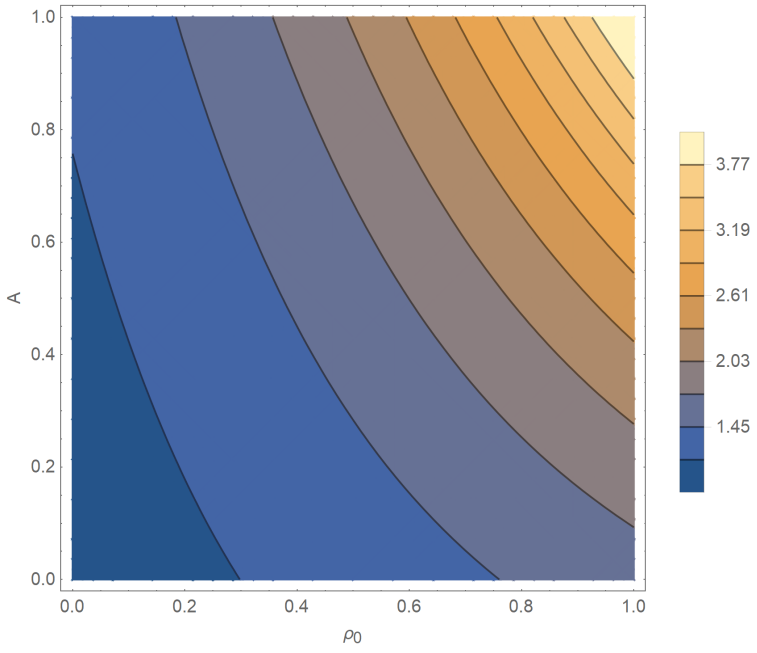

Figure 3.3: Contour plot of the proper radius b as a function of parameters A and ρ_0.

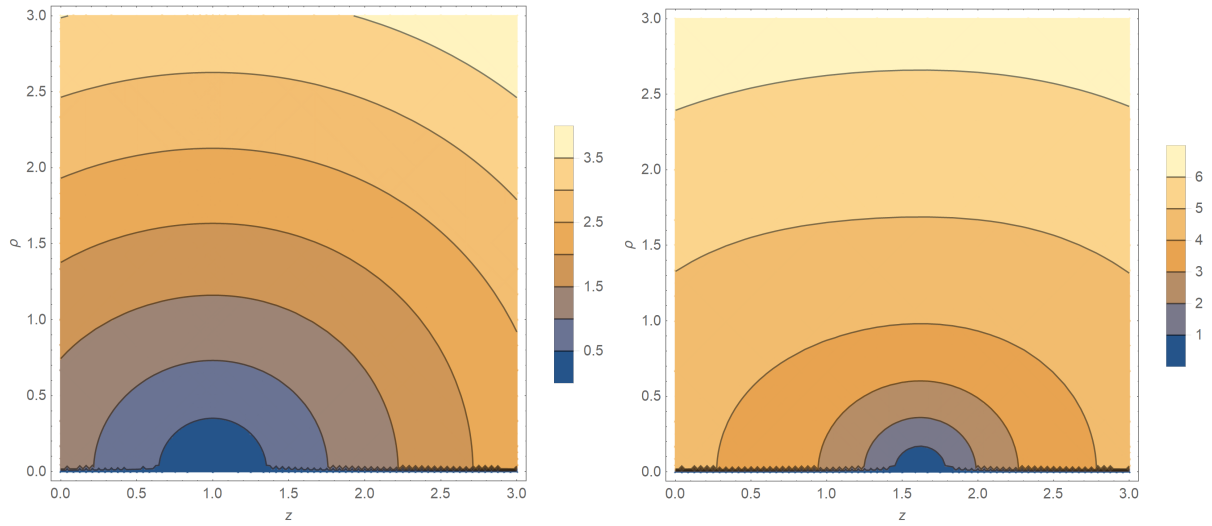

Figure 3.4: Proper distance from the "ring" in the same meridional plane for $A = 1$, $\rho_0 = 0$ (left) and $\rho_0 = 1$ (right).

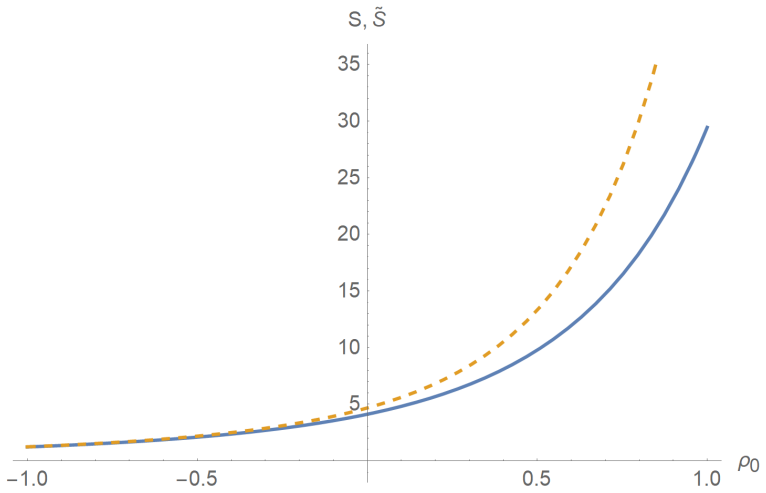

Figure 3.5: Proper area S (solid line) and Euclidean area $\tilde{S}$ (dashed line) as a function of ρ_0.

3.5 Limit $\rho_{\max} \to 0^+$

This limit corresponds to the Euclidean radius of the "ring" in the Brill metric going to zero.

In our case the $\rho_{\max} \to 0^+$ limit due to (1.7) is equivalent to $\rho_0 \to -\infty$. In this limit the space part of the metric (1.1) becomes

$$\mathrm{d}l^2 = \mathrm{d}\rho^2 + \rho^2 \mathrm{d}\phi^2 + \mathrm{d}z^2, \tag{3.9}$$

which is three metric of a 3D Euclidean space in cylindrical coordinates. From here we trivially get

$$\begin{aligned} l &= 0, \\ L &= 2\pi\rho_{\max} = 0, \\ r &= \int_0^{\rho_{\max}} \mathrm{d}\rho = 0, \\ d &= \left| \int_0^{\frac{\tilde{z}}{\sin\alpha}} n^\mu n_\mu \, \mathrm{d}k \right| \overset{\|n\|=1}{=} \frac{\tilde{z}}{\sin\alpha} = \sqrt{\tilde{z}^2 + \tilde{\rho}^2}, \\ S &= 2\pi \int_0^{\rho_{\max}} \rho \, \mathrm{d}\rho = 0. \end{aligned} \tag{3.10}$$

We shall see in Section 5.2 that the total mass-energy of a static "snapshot" of the Brill wave is zero and therefore one would not expect the above limit to produce any singularity. The thin-ring sources behave very differently since they carry mass and thus their singularity can be expected. All of the ring sources which we consider in this thesis exhibit extreme behavior in this limit (see Table 2.1).

4. Conformal transformation

We will not be discussing the time evolution of the Brill solution in this thesis. However, we will outline some of the basic methods used as they will prove useful in the following discussion (see Appendix B).

As mentioned in Chapter 1, the metric (1.1) can be conformally rescaled such that it has vanishing scalar curvature $\overline{R}^{i}{}_{i}$. The new form of the metric is then given as

$$\gamma_{ij} = \psi^4 \overline{\gamma}_{ij}, \tag{4.1}$$

where ψ is the conformal factor. The Hamiltonian constraint then takes the form

$$\nabla^2 \psi - \frac{1}{8}\, {}^3\overline{R}\psi = 0, \tag{4.2}$$

where ${}^3\overline{R}$ is the spatial part of the Ricci scalar curvature associated with theconformally transformed 3−metric $\overline{\gamma}_{ij}$. We will calculate the scalar curvature from the Riemann tensor, which is given by

$$\overline{R}^{l}{}_{mns} = -\overline{\Gamma}^{l}{}_{mn,s} + \overline{\Gamma}^{l}{}_{ms,n} + \overline{\Gamma}^{e}{}_{ms}\overline{\Gamma}^{l}{}_{en} - \overline{\Gamma}^{e}{}_{mn}\overline{\Gamma}^{l}{}_{es}, \tag{4.3}$$

where $\overline{\Gamma}^{l}{}_{mn}$ are the Christoffel symbols associated with a given 3-metric (1.1) by

$$\overline{\Gamma}^{l}{}_{mn} = \frac{1}{2}\overline{\gamma}^{ls}\left(\overline{\gamma}_{sn,m} - \overline{\gamma}_{mn,s} + \overline{\gamma}_{sm,n}\right). \tag{4.4}$$

Nontrivial Christoffel symbols for the metric given by (1.1) are listed in Appendix A, Eq. (7.23).

The Ricci tensor is given as a contraction over the first and third index of the Riemann tensor

$$\overline{R}_{ij} = \overline{R}^{k}{}_{ikj}. \tag{4.5}$$

The scalar curvature is in turn defined as a contraction of the Ricci tensor,

$${}^3\overline{R} = \overline{R}^{i}{}_{i} = \overline{\gamma}^{ij}\overline{R}_{ji}, \tag{4.6}$$

which comes out to be

$${}^3\overline{R} = -2e^{-2q(\rho,z)}[q_{,zz}(\rho,z) + q_{,\rho\rho}(\rho,z)]. \tag{4.7}$$

Figure 4.1 (left) shows the Ricci scalar for $A = 1$ and $\rho_0 = 0$ along the ρ-axis. It does not reach its maximum on a "ring" in the equatorial plane. For the above choise of parametrs the maximum occurs at

$$\rho \doteq 0.87.$$

Figure 4.1 (right) also shows the maxium of the radial part of the 3-Ricci scalar ${}^3\overline{R}$ and the coordinate "ring" radius $\rho_{\max}$ along the ρ-axis as a function of the parameter ρ_0. Both approach zero since for $\rho_0 \to -\infty$ the space becomes flat (see Section 3.5). We also note that

numerical plotting shows that the scalar curvature develops two local maxima at $\rho_0 \doteq 0.79$. The maximum in Figure 4.1 is the global maximum corresponding to lower values of the cylindrical radius ρ.

Using (4.7) Eq. (4.2) becomes

$$\nabla^2\psi + \frac{1}{4}e^{-2q(\rho,z)}[q_{,zz}(\rho,z) + q_{,\rho\rho}(\rho,z)]\psi = 0. \tag{4.8}$$

For the seed function given by (1.2) Eq. (4.2) becomes

$$\nabla^2\psi + \frac{A}{2}\left(2\rho^4 + 2\rho^2\rho_0^2 - 4\left(\rho^2 - 1\right)\rho\rho_0 + 2\rho^2\left(z^2 - 3\right) + 1\right) \exp\left[-2A\rho^2 e^{-(\rho_0-\rho)^2 - z^2} - (\rho_0 - \rho)^2 - z^2\right]\psi = 0, \tag{4.9}$$

where the flat Laplace operator in cylindrical coordinates takes the form

$$\nabla^2 = \frac{\partial^2}{\partial\rho^2} + \frac{1}{\rho}\frac{\partial}{\partial\rho} + \frac{\partial^2}{\partial z^2}. \tag{4.10}$$

This equation has no known analytical solutions. However, it can be solved numerically by means of pseudo-spectral method, i.e., by writing the conformal factor as [3, 4]

$$\psi(\rho, z) = 1 + \sum_{i=1}^{N_\rho}\sum_{j=1}^{N_z} a_{ij} SB_i(\rho) SB_j(z), \tag{4.11}$$

where N_i is the number of grid points in the i-direction, a_{ij} are the unknown coefficients and $SB_i(x)$ are the "rational Chebyshev functions" given by

$$SB_i(x) = \sin\left((i+1)\operatorname{arccot}\left(\frac{x}{L_x}\right)\right), \tag{4.12}$$

where L_x is the mapping parameter along x-axis. The numerical solution of (4.9) itself goes beyond the scope of this thesis.

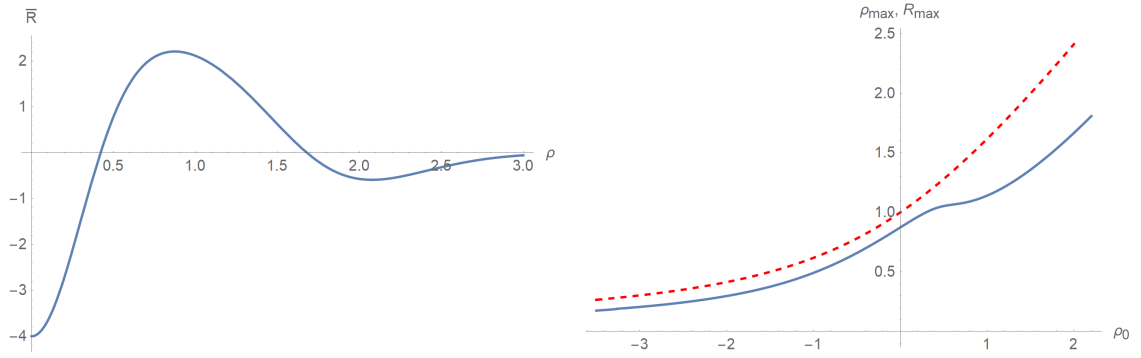

Figure 4.1: 3D Ricci scalar (4.7) for $A = 1$ and $\rho_0 = 0$ along the ρ-axis [left figure], and maximum of the radial part of the 3-Ricci scalar ${}^3\overline{R}$ (solid line) and the coordinate "ring" radius $\rho_{\max}$ (dashed line)[right figure].

5. Static solution

The Brill waves are vacuum axially symmetric solution of Einstein equations. However, it is not a static solution. The time evolution of Brill waves is rather complicated and we will not discuss it in this thesis[1]. We will instead fix the space metric (1.1) and consider the solution static. This can be justified if one studies the wave near the moment of time symmetry only for a short amount of time. Keeping the solution static would require a certain nontrivial source $T_{\mu\nu}$ which we will discuss in Section 5.2.

5.1 General form of the Weyl metric

The Brill solution at the moment of time symmetry is given in so called Weyl canonical coordinates. It can be shown that if the space-time is static and axially symmetric with the energy-momentum tensor satisfying the condition [5]

$$T^{\rho}_{\ \rho} + T^{z}_{\ z} = 0, \tag{5.1}$$

then the complete 4-metric can be written in terms of two functions A and B as

$$\mathrm{d}s^2 = -e^{2A}\mathrm{d}t^2 + e^{2(B-A)}(\mathrm{d}\rho^2 + \mathrm{d}z^2) + e^{-2A}\rho^2\mathrm{d}\phi^2. \tag{5.2}$$

This static Brill solution is not vacuum for the reasons mentioned above, so the condition (5.1) is not automatically satisfied. However, we shall see in Section 5.2 that the condition (5.1) is met.

Comparing (1.1) to (5.2) we get

$$\begin{aligned} A &= 0, \\ B &= q(\rho, z), \end{aligned} \tag{5.3}$$

and thus the full metric of the Brill wave in the fixed moment of time symmetry can be written as

$$\mathrm{d}s^2 = -\mathrm{d}t^2 + e^{2q(\rho,z)}(\mathrm{d}\rho^2 + \mathrm{d}z^2) + \rho^2\mathrm{d}\phi^2. \tag{5.4}$$

The space-time exhibits two Killing symmetries

$$\begin{aligned} \eta^{\mu} &= (1, 0, 0, 0), \\ \xi^{\mu} &= (0, 0, 0, 1). \end{aligned} \tag{5.5}$$

5.1.1 Curvature of the equatorial plane

The Gauss curvature is an important invariant giving insight into the geometry of a given surface in the space-time. We are going to be mainly interested in the curvature of the equatorial plane $\{t = \text{const.},\ z = 0\}$ where the "ring" is situated. The Gauss curvature is

[1] The papers concerning the time evolution of Brill waves include [3, 4, 6], for example.

defined as half of the corresponding Ricci scalar. For the equatorial plane and the general form of Weyl metric (5.2) the 2-dimensional Ricci scalar is

$$\frac{^2R}{2} = G^{\text{eq.}} = -\frac{2e^{2(A(\rho,0)-B(\rho,0))}\left(A_{,\rho}(\rho,0)\left(\rho B_{,\rho}(\rho,0)-1\right)-\rho A_{,\rho\rho}(\rho,0)-B_{,\rho}(\rho,0)\right)}{\rho}. \quad (5.6)$$

Using (5.3) and (1.2) we get

$$G^{\text{eq.}} = \frac{e^{-2q(\rho,0)}q_{,\rho}(\rho,0)}{\rho} = -4A\left(\rho_0\rho-\rho^2-1\right)\exp\Big[(\rho-\rho_0)^2-2A\rho^2e^{(\rho-\rho_0)^2}\Big]. \quad (5.7)$$

Figure 5.1 shows the Gauss curvature of the equatorial plane as a function of the cylindrical radius ρ for $A = 1$ and $\rho_0 = 0$. For $A > 0$ the Gauss curvature reaches its maximum of $4Ae^{\rho_0^2}$ at the origin and the plane is asyptotically flat. For negative values of the amplitude the bavior of the Gauss curvature near the origin depends on the choice of the parameter ρ_0, however, the solution asyptotically approaches negative infinity $\forall\rho_0 \in \mathbb{R}$. This is not analogous to any of the ring sources considered above as the Gauss curvature vanishes at the radial infinity for all the ring sources.

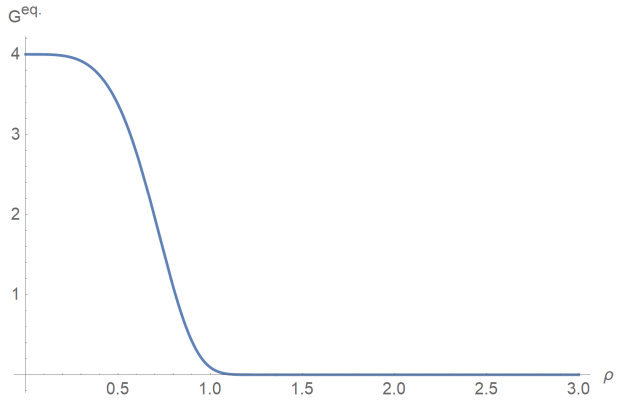

Figure 5.1: The Gauss curvature of the equatorial plane for $A = 1$ and $\rho_0 = 0$. See figure 6 in [1] for the Gauss curvature of the thin-rings.

5.1.2 Kretschmann scalar

Having now derived the full form of the metric in the static case, we can evaluate some of its 4-dimensional invariants that can reveal potential singularities in the space-time. One of the most commonly used is the Kretschmann scalar

$$K \equiv R^{\mu\nu\iota\sigma}R_{\mu\nu\iota\sigma}, \quad (5.8)$$

where $R_{\mu\nu\iota\sigma}$ is the covariant Riemann tensor given by (4.3). For the metric (5.4) the Kretschmann scalar is given by a quite long formula which reduces to

$$K = 16A^2(4\rho^8+8\rho^6(z^2-3)+2\rho^2(3z^2-8)+\rho^4(4z^4-24z^2+42)+3) \exp\Big[-2(2A\rho^2e^{-\rho^2-z^2}+\rho^2+z^2)\Big], \quad (5.9)$$

for $\rho_0 = 0$. The Kretschmann scalar is everywhere finite and asymptotically (at radial infinity) goes to zero $\forall A, \rho_0 \in \mathbb{R}$. Figure 5.2 shows the Kretschmann scalar in the meridional plane for different choices of the parameters A and ρ_0. For $\rho_0 = 0$, K reaches its maximum at the origin. This is in agreement with [6] who observed that the maximum even stays at the origin during the time evolution.

The Kretschmann scalar for all the thin-ring sources diverges (at least from a certain direction) at the ring itself showing the singular character of the thin rings. For the M-P ring, the behavior of the Kretschmann scalar does not depend on the direction in which the ring is approached which is also true for the Brill solution. The other rings are strongly directional. We shall see that a different choice of the seed function can resolve in a similar directional behavior in Section 6.

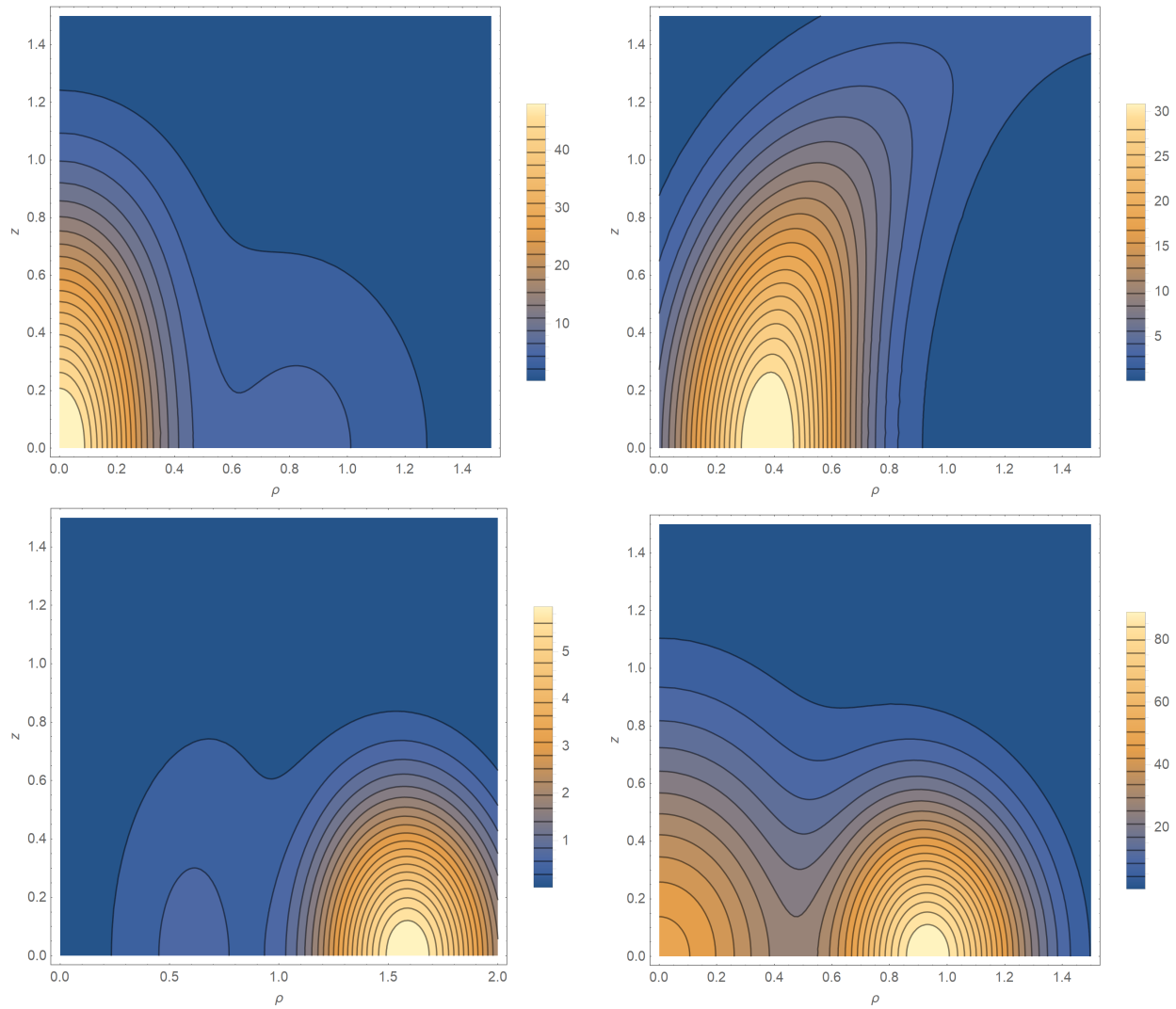

Figure 5.2: The Kretschmann scalar in the meridional plane for the values of parameters $[A, \rho_0]$: $[1, 0]$ (top left), $[1, 1]$ (top right), $[-0.1, 1]$ (bottom left) and $[-1, 0]$ (bottom right). See figures 8 and 9 in [1] for the Kretschmann scalar within the meridional plane for the thin-rings.

5.2 Energy-momentum tensor

As mentioned above, the static metric given by (5.4) is not a vacuum solution. In this Section we will evaluate the energy-momentum tensor $T_{\mu\nu}$ using Einstein's equations with the above metric.

Using (4.3), (4.4) and (4.5) with the metric given by (5.4), the Ricci tensor in the (t, ρ, z, ϕ) basis reads

$$R_{\mu\nu} = \begin{pmatrix} 0 & 0 & 0 & 0 \\ 0 & \frac{1}{\rho}\frac{\partial q(\rho,z)}{\partial \rho} - \frac{\partial^2 q(\rho,z)}{\partial z^2} - \frac{\partial^2 q(\rho,z)}{\partial \rho^2} & \frac{1}{\rho}\frac{\partial q(\rho,z)}{\partial z} & 0 \\ 0 & \frac{1}{\rho}\frac{\partial q(\rho,z)}{\partial z} & -\frac{1}{\rho}\frac{\partial q(\rho,z)}{\partial \rho} - \frac{\partial^2 q(\rho,z)}{\partial z^2} - \frac{\partial^2 q(\rho,z)}{\partial \rho^2} & 0 \\ 0 & 0 & 0 & 0 \end{pmatrix}, \tag{5.10}$$

and the scalar curvature is again given by

$$R \;=\; {}^3\overline{R} \;=\; -2e^{-2q(\rho,z)}\left(\frac{\partial^2 q(\rho,z)}{\partial z^2} + \frac{\partial^2 q(\rho,z)}{\partial \rho^2}\right).$$

The Einstein tensor, given by

$$G_{\mu\nu} \stackrel{\text{def.}}{=} R_{\mu\nu} - \frac{1}{2} R g_{\mu\nu}, \tag{5.11}$$

thus takes the form

$$G_{\mu\nu} = \begin{pmatrix} -e^{-2q(\rho,z)}\left(\frac{\partial^2 q(\rho,z)}{\partial z^2} + \frac{\partial^2 q(\rho,z)}{\partial \rho^2}\right) & 0 & 0 & 0 \\ 0 & \frac{1}{\rho}\frac{\partial q(\rho,z)}{\partial \rho} & \frac{1}{\rho}\frac{\partial q(\rho,z)}{\partial z} & 0 \\ 0 & \frac{1}{\rho}\frac{\partial q(\rho,z)}{\partial z} & -\frac{1}{\rho}\frac{\partial q(\rho,z)}{\partial \rho} & 0 \\ 0 & 0 & 0 & e^{-2q(\rho,z)}\rho^2\left(\frac{\partial^2 q(\rho,z)}{\partial z^2} + \frac{\partial^2 q(\rho,z)}{\partial \rho^2}\right) \end{pmatrix}. \tag{5.12}$$

Using Einstein equations without the cosmological constant

$$G_{\mu\nu} = 8\pi T_{\mu\nu}, \tag{5.13}$$

we get

$$T_{\mu\nu} = \frac{1}{8\pi}\begin{pmatrix} -e^{-2q(\rho,z)}\left(\frac{\partial^2 q(\rho,z)}{\partial z^2} + \frac{\partial^2 q(\rho,z)}{\partial \rho^2}\right) & 0 & 0 & 0 \\ 0 & \frac{1}{\rho}\frac{\partial q(\rho,z)}{\partial \rho} & \frac{1}{\rho}\frac{\partial q(\rho,z)}{\partial z} & 0 \\ 0 & \frac{1}{\rho}\frac{\partial q(\rho,z)}{\partial z} & -\frac{1}{\rho}\frac{\partial q(\rho,z)}{\partial \rho} & 0 \\ 0 & 0 & 0 & e^{-2q(\rho,z)}\rho^2\left(\frac{\partial^2 q(\rho,z)}{\partial z^2} + \frac{\partial^2 q(\rho,z)}{\partial \rho^2}\right) \end{pmatrix}. \tag{5.14}$$

Using this form of the energy-momentum tensor, Eq. (5.1) reads

$$T^{\rho}_{\ \rho} + T^{z}_{\ z} = \frac{e^{-2q(\rho,z)}}{8\pi}\frac{1}{\rho}\frac{\partial q(\rho,z)}{\partial \rho} - \frac{e^{-2q(\rho,z)}}{8\pi}\frac{1}{\rho}\frac{\partial q(\rho,z)}{\partial \rho} = 0, \tag{5.15}$$

so the derivation in Section 5.1 is consistent and the metric (5.4) is really the Weyl-type metric.

As the system is closed we require $T^{\mu\nu}{}_{;\nu} = 0$ where the comma stands for a covariant derivative defined as

$$\tau^{\mu\nu}{}_{;\iota} = \tau^{\mu\nu}{}_{,\iota} + \Gamma^{\mu}{}_{\iota\sigma}\tau^{\sigma\nu} + \Gamma^{\nu}{}_{\iota\sigma}\tau^{\mu\sigma}, \tag{5.16}$$

where $\Gamma^{\mu}{}_{\nu\iota}$ are the Christoffel symbols given by (4.4).

For the Killing coordinates the condition is met trivially. The other two conditions are also met, regardless of the choice of the seed function. In fact, since the above conditions restrict only the source $T_{\mu\nu}$, any source obtained from Einstein's equations (5.13) by the procedure above automatically satisfies the covariant divergence conditions $T^{\mu\nu}{}_{;\nu} = 0$.

5.2.1 Invariants of the energy-momentum tensor

One of the important invariants we will focus on is the trace $T^{\mu}{}_{\mu}$ of the associated energy-momentum tensor. Due to the Weyl condition (5.15), the trace reduces to the sum over the two Killing coordinates,

$$T \equiv T^{\mu}{}_{\mu} \overset{(5.15)}{=} T^{t}{}_{t} + T^{\phi}{}_{\phi} = \frac{q_{,\rho\rho}(\rho,z) + q_{,zz}(\rho,z)}{4\pi}\, e^{-2q(\rho,z)} = \\ \frac{A[2\rho_0^2\rho^2 - 4\rho_0(\rho^2-1)\rho + 2\rho^4 + 2\rho^2(z^2-3)+1]}{2\pi} \exp\Big[-2A\rho^2 e^{-(\rho_0-\rho)^2-z^2} - (\rho_0-\rho)^2 - z^2\Big]. \tag{5.17}$$

The trace is thus everywhere finite and vanishes at radial infinity. Due to Einstein's equations (5.13) the trace of the energy-momentum tensor is proportional to the Ricci scalar

$$R = -T, \tag{5.18}$$

so the minima of the trace T correspond to maxima of the Ricci scalar discussed in the previous Chapter 4 (see Figure 4.1). For the negative values of A, the position of the extreme is different. Figure 5.3 shows the position of the extreme near the "ring" (maximum/minimum for negative/positive values of the amplitude respectively). It also compares it with the "ring" coordinate radius $\rho_{\max}$. We can see that the solution with negative amplitudes behaves as we would expect (Ricci scalar has an extreme on the "ring") for high values of the parameter ρ_0 despite the unintuitive features of this solution discussed above.

For $\rho_0 = 0$ and positive values of the amplitude A, the trace reaches its maximum of $\frac{A}{2\pi}$ at the origin. Figure 5.4 shows the trace T for $A = \pm 1$ in the meridional plane.

Due to the two existing Killing symmetries, the T_{tt} and $T_{\phi\phi}$ components of the energy-momentum tensor are invariants of the space-time. Let us focus of the time component

$$T_{tt} = T_{\mu\nu}\eta^{\mu}\eta^{\nu} = -\frac{e^{-2q(\rho,z)}}{8\pi}\left(\frac{\partial^2 q(\rho,z)}{\partial z^2} + \frac{\partial^2 q(\rho,z)}{\partial \rho^2}\right), \tag{5.19}$$

whose physical meaning is the local mass-energy density present in the space-time measured by a static observer. The total mass-energy enclosed in a volume V is given by the volume integral of the density

$$E_V = \int_V T_{tt}\, \mathrm{d}V = -2\pi \int_{V(\rho,z)} \frac{e^{-2q(\rho,z)}}{8\pi}\left(\frac{\partial^2 q(\rho,z)}{\partial z^2} + \frac{\partial^2 q(\rho,z)}{\partial \rho^2}\right)\rho\, \mathrm{d}\rho\, \mathrm{d}z. \tag{5.20}$$

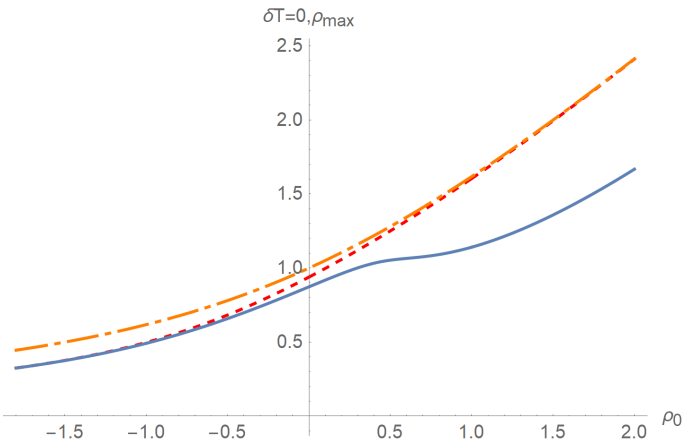

Figure 5.3: Position of the extreme of the energy-momentum tensor trace - minimum for positive A, (solid line), maximum for negative A (dashed line) and the "ring" coordinate radius $\rho_{\max}$ (dot-dashed line).

Using the seed function (1.2) and selecting a special form of V to be a cylinder with radius k and height of $2k$ centered at the origin we get

$$E_V(k) = -\frac{1}{2}A\int_{-k}^{k}\int_{0}^{k}\rho\left(2\rho^4+2\rho^2\left(z^2-3\right)+1\right)\exp\left[\rho^2(-2Ae^{-\rho^2-z^2}-1)-z^2\right]\,\mathrm{d}\rho\,\mathrm{d}z. \tag{5.21}$$

Figure 5.5 shows the numerical evaluation of the energy E_V as a function of the parameter k. The mass-energy enclosed in the entire space (i.e. $k\to\infty$) for $A=1$ is then

$$E_V(k\to\infty)\doteq 0.173.$$

The total mass-energy $E_V(k\to\infty)$ is shown in Figure 5.5 as a function of the amplitude A. Let us note that $E_V(k\to\infty)=0$ for $A=0$ as that corresponds to empty space.

Because in the static case $T_{\phi\phi}=T_{tt}$, the trace of the energy-momentum tensor can also be thought of as twice the mass-energy density in the space-time. We can see from the Figure 5.4 that there are areas in which the mass-energy density T_{tt} is positive and negative. This violates the weak energy condition, which states that for every time like vector field u^μ the term

$$T_{\mu\nu}u^\mu u^\nu,$$

is non-negative which is not true in our case (consider for example $u^\mu=\eta^\mu$). The weak energy condition is usually considered met "automatically" in most "physically meaningful" solution of general relativity as its violation indicates the potential existence of closed time-like curves.

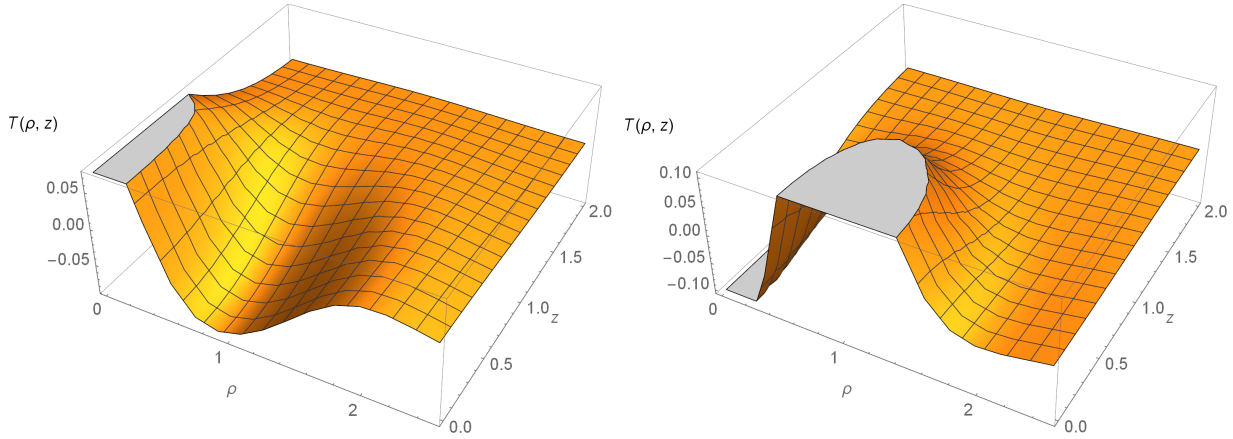

Figure 5.4: The trace of the energy-momentum tensor T with $\rho_0 = 0$, $A = 1$ (left) and $A = -1$ (right).

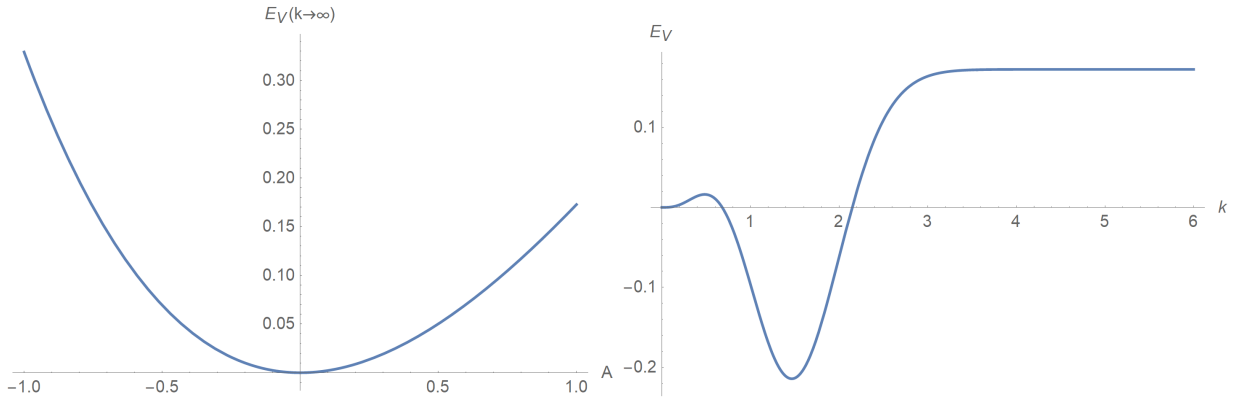

Figure 5.5: Energy E_V enclosed in a cylinder V as a function of its radius and half-height (left) and the total mass-energy in the whole space as a function of the measure of amplitude A (right).

5.2.2 Total mass-energy of the wave

In the previous Subsection we have presented the formula (5.21) for the mass-energy enclosed in a volume V of the space-time which along with the "gravitational" energy adds up to the total mass-energy of the wave. The "gravitation" energy is not defined in a satisfying manner and so we will focus on the total mass-energy of the space-time which is more relevant to us as it impacts the asymptotic behavior (1.6) of the conformal factor. We will use the Tolman integral [7] which gives the mass-energy of volume V of space as

$$m = \int_V (T^{\mathrm{i}}_{\mathrm{i}} - T^{\mathrm{t}}_{\mathrm{t}})\sqrt{-g}\ \mathrm{d}^3x, \tag{5.22}$$

where $\sqrt{-g}$ is the square root of the determinant of the covariant metric. Using the general result (5.14) and Weyl form of the metric (5.4) we get

$$T^i_i - T^t_t \overset{(5.15)}{=} T^\phi_\phi - T^t_t = 0, \tag{5.23}$$

and thus the mass-energy of any volume of space is zero. Using the results given by (5.19) we can conclude that the "gravitational" energy is negative. This is plausible as one would expect the "binding" energy to be negative.

The mass m determining the asymptotic behavior of the conformal factor (1.6) equals the Tolman mass. For a more thorough proof of $m = 0$ using the second form of the seed function discussed in Section 6, see Appendix B.

6. Second form of the seed function

In this Chapter we will focus on a less commonly used form of the seed function, given in cylindrical coordinates as [4]

$$q(\rho, z) = a\frac{\rho^2}{1 + \left(\frac{\sqrt{z^2+\rho^2}}{\lambda}\right)^n}, \qquad n \geq 4, \tag{6.1}$$

where a is a dimensionless measure of the amplitude, λ measure of wavelength with the units of length and n determines the asymptotic behavior of the seed function. The $n \geq 4$ condition is imposed so that q falls of as $\sim \frac{1}{r^2}$ as $r \to \infty$ or faster which is a general condition that the seed function should meet. We note that this choice of the seed function satisfies $q(0, z) = q_{,\rho}(0, z) = 0$, and is thus a viable choice.

Once again we calculate the position of a maximum of the metric where the imaginary "ring" would lie. In order to do that we take derivative of the radial metric element along the $z = 0,\ \phi = \text{const.}$ semi-line,

$$0 = \frac{\partial e^{q(\rho,0)}}{\partial \rho} = a\rho\frac{2(1 + (\frac{\rho}{\lambda})^n) - \rho\frac{n\rho^{n-1}}{\lambda^n}}{(1 + (\frac{\rho}{\lambda})^n)^2}e^{q(\rho,0)} = a\rho\frac{2 + (2 - n)(\frac{\rho}{\lambda})^n}{(1 + (\frac{\rho}{\lambda})^n)^2}e^{q(\rho,0)},$$

which has only one nontrivial solution

$$\rho_{\max} = \left(\frac{2}{n-2}\right)^{\frac{1}{n}}\lambda. \tag{6.2}$$

Figure 6.1 shows the maximum of the radial metric $\rho_{\max}$ as a function of n for a fixed parameter $\lambda = 1$. We note that it is everywhere positive; the limit $\rho_{\max} \to 0^+$ can only be achieved for $\lambda \to 0^+$. If we focus on the limiting cases we trivially get

$$\lim_{n\to 4}\rho_{\max}(n, \lambda) = \lim_{n\to 4}\left(\frac{2}{n-2}\right)^{\frac{1}{n}}\lambda = \lambda,$$

and

$$\lim_{n\to \infty}\rho_{\max}(n, \lambda) = \lim_{n\to \infty}\left(\frac{2}{n-2}\right)^{\frac{1}{n}}\lambda = \lambda. \tag{6.3}$$

We will now focus on the invariant properties of the "ring" which for the first form of the seed function have already been computed above. Firstly, we will convert the seed function to spherical coordinates using the standard transformation

$$\begin{aligned} x &= r\cos\phi\ \sin\theta, \\ x &= r\sin\phi\ \sin\theta, \\ z &= r\sin\phi, \end{aligned}$$

yielding

$$q(r, \theta) = a\frac{r^2\cos^2\theta}{1 + (\frac{r}{\lambda})^n}, \tag{6.4}$$

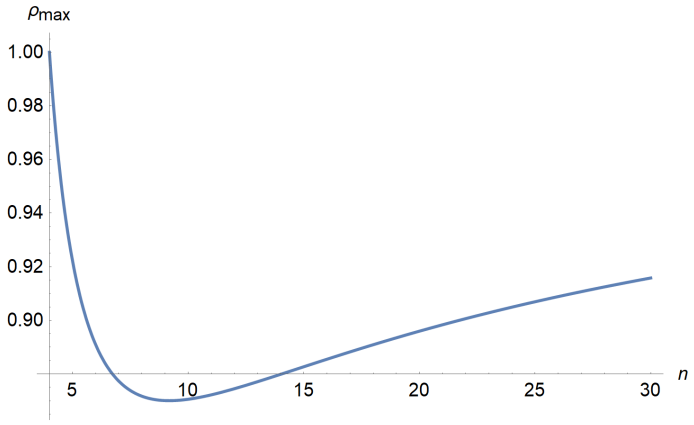

Figure 6.1: Maximum of the radial metric $\rho_{\max}$ for $\lambda = 1$ as a function of the parameter n.

and to toroidal coordinates given by (1.8) with $\rho_{\max}$ given by (6.2), which yields

$$q(\zeta, \psi) = a \frac{\rho_{\max}^2 \frac{\sinh^2 \zeta}{(\cosh \zeta - \cos \psi)^2}}{1 + (\frac{\rho_{\max}}{\lambda} \frac{\sqrt{\sinh^2 \zeta + \sin^2 \zeta}}{\cosh \zeta - \cos \psi})^n}. \tag{6.5}$$

6.1 Small and large circumference

Following the same procedure as in Section 3.1 we get for the small circumference

$$l = \lim_{k \to \infty} \oint \sqrt{g_{\psi\psi}(k, \phi, \psi)} \, \mathrm{d}\psi = \lim_{k \to \infty} \int_0^{2\pi} \rho_{\max} \frac{e^{q(k,\psi)}}{\cosh k - \cos \psi} \, \mathrm{d}\psi.$$

Just as before the integrand is continuous and thus finite $\forall k \in \mathbb{R}^+$ and we can use the continuous dependence of an integral on a parameter theorem and get

$$l = \rho_{\max} \int_0^{2\pi} \lim_{k \to \infty} \frac{e^{q(k,\psi)}}{\cosh k - \cos \psi} \, \mathrm{d}\psi,$$

where

$$\lim_{k \to \infty} e^{q(k,\psi)} = \exp\left[\frac{a \rho_{\max}^2}{1 + (\frac{\rho_{\max}}{\lambda})^n} \right] = \text{const.},$$

and thus we get $l = 0$ again. This result shows that the metric does not behave too wildly near the imaginary "ring".

As noted in Section 3.2, the large circumference L comes out the same

$$L = 2\pi \rho_{\max},$$

as it does not depend on the choice of the seed function.

6.2 Proper radius

Proper radius of the "ring" is again given by

$$b(a,\lambda,n) = \int_0^{\rho_{\max}} \sqrt{g_{\rho\rho}(\rho,0)}\ \mathrm{d}\rho = \int_0^{\rho_{\max}} \exp\left[a\frac{\rho^2}{1+(\frac{\rho}{\lambda})^n}\right]\ \mathrm{d}\rho. \tag{6.6}$$

This integral can be computed numerically. The proper radius is a monotonically increasing function of the parameters $a > 0$ and λ. To show that we take the respective derivatives. The proper radius does not depend on the parameter n in this simple way. We will discuss it later in this Section. For a we simply get

$$\frac{\partial b}{\partial a} = \frac{\partial}{\partial a}\int_0^{\rho_{\max}} \exp\left[a\frac{\rho^2}{1+(\frac{\rho}{\lambda})^n}\right]\ \mathrm{d}\rho = \int_0^{\rho_{\max}} \frac{\partial}{\partial a}\exp\left[a\frac{\rho^2}{1+(\frac{\rho}{\lambda})^n}\right]\ \mathrm{d}\rho = \int_0^{\rho_{\max}} \frac{\rho^2}{1+(\frac{\rho}{\lambda})^n}\exp\left[a\frac{\rho^2}{1+(\frac{\rho}{\lambda})^n}\right]\ \mathrm{d}\rho \geq 0,$$

as the integrand is positive on $(0,\rho_{\max})$. The equality only holds in the trivial case $\rho_{\max} = 0$ i.e. $\lambda = 0$.

Similarly,

$$\frac{\partial b}{\partial \lambda} = \frac{\partial}{\partial \lambda}\int_0^{\rho_{\max}} \exp\left[a\frac{\rho^2}{1+(\frac{\rho}{\lambda})^n}\right]\ \mathrm{d}\rho = \int_0^{\rho_{\max}} \frac{\partial \exp\left[a\frac{\rho^2}{1+(\frac{\rho}{\lambda})^n}\right]}{\partial\lambda}\ \mathrm{d}\rho + \exp\left[a\frac{\rho_{\max}^2}{1+(\frac{\rho_{\max}}{\lambda})^n}\right]\frac{\partial\rho_{\max}}{\partial\lambda} =$$
$$\int_0^{\rho_{\max}} \frac{na\rho^2}{(1+(\frac{\rho}{\lambda})^n)^2}\frac{\rho^n}{\lambda^{n+1}}\exp\left[a\frac{\rho^2}{1+(\frac{\rho}{\lambda})^n}\right]\ \mathrm{d}\rho + \exp\left[a\frac{\rho_{\max}^2}{1+(\frac{\rho_{\max}}{\lambda})^n}\right](\frac{2}{n-2})^{\frac{1}{n}} > 0, \tag{6.7}$$

where the first term is non-negative for positive values of the amplitude a and is only zero in the trivial case $\rho_{\max} = 0 \implies \lambda = 0$. The second term is always positive and thus the sum is positive for $a > 0$. For negative amplitudes the inequality (6.7) does not generally hold. However, we can show that it holds on some neighbourhood of $a = 0$. For zero amplitude the derivative reduces to

$$\frac{\partial b}{\partial \lambda} = \left(\frac{2}{n-2}\right)^{\frac{1}{n}} > 0,$$

which was shown above (see Figure 6.1). The derivative is also a continuous function of the amplitude so there exist $\delta > 0$ such that $\frac{\partial r}{\partial\lambda} > 0,\ \forall a \in (-\delta,\infty)$. Figure 6.2 shows the derivative of the proper radius with respect to λ for $n = 4$ and $\lambda = 1$ as a function of a. For this choise of the parameters the local extreme of the proper radius with respect to λ occurs at $a \doteq -3.53$.

The dependence $b = b(n)$ is more complicated as we can also see from Figure 6.1 since the maximum of the radial metric $\rho_{\max}$ is not a monotonically increasing function of n. Figure 6.3 shows the proper radius as a function of n and its inverse for fixed parameters $\lambda = 1$ and $a = 1$. As noted above, in the $n \to \infty$ limit the radius of the "ring" $\rho_{\max}$ approaches unity. Thus for fixed parameters $\lambda = 1$ and $a = 1$ we get

$$\lim_{n\to\infty} b(1,1,n) = \lim_{n\to\infty}\int_0^{\rho_{\max}} e^{\frac{\rho^2}{1+\rho^n}}\ \mathrm{d}\rho = \int_0^1 e^{\rho^2}\ \mathrm{d}\rho, \tag{6.8}$$

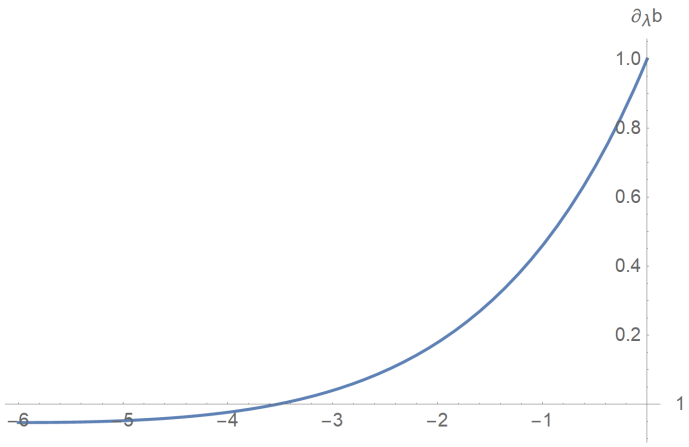

Figure 6.2: The derivative of the proper radius with respect to λ for $n = 4$ and $\lambda = 1$ for negative values of the amplitude a.

which can be solved numerically[1]

$$\lim_{n\to\infty} b(1, 1, n) \doteq 1.46,$$

in agreement with Figure 6.3.

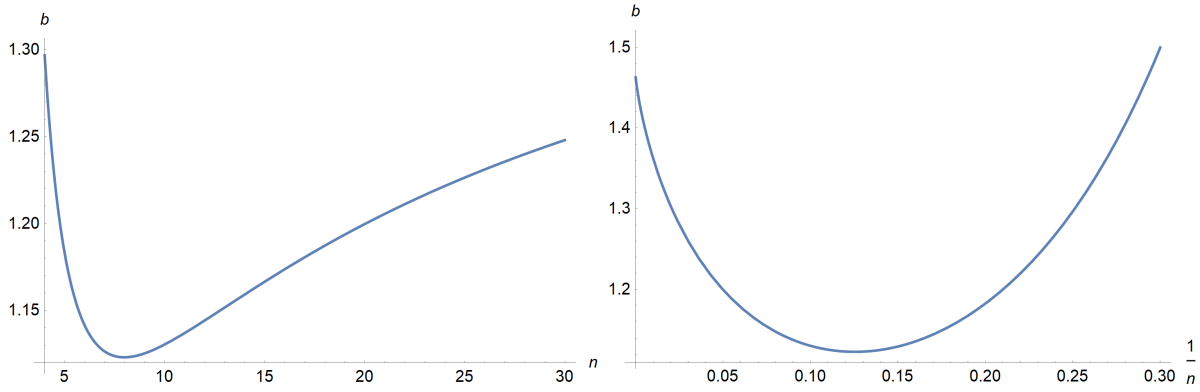

Figure 6.3: Proper radius b for the seed function given by (6.1) with $\lambda = 1$ and $a = 1$ as a function of n and its inverse.

[1]This result is given in some arbitrary units of length determined by λ.

6.3 Proper distance

Let us now focus on the proper distance from the "ring" to an arbitrary point in the same meridional plane. It is convenient to show first that the measure of amplitude a and wavelength λ are not independent. Let us perform a change of coordinates according to

$$\begin{aligned} \rho &= \lambda\tilde{\rho}, \\ z &= \lambda\tilde{z}. \end{aligned} \tag{6.9}$$

the seed function becomes

$$q(\tilde{\rho},\tilde{z}) = a\lambda^2 \frac{\tilde{\rho}^2}{1+(\tilde{z}^2+\tilde{\rho}^2)^{\frac{n}{2}}} \overset{\text{def.}}{=} \Lambda \frac{\tilde{\rho}^2}{1+(\tilde{z}^2+\tilde{\rho}^2)^{\frac{n}{2}}}, \quad n \geq 4, \tag{6.10}$$

where $\Lambda \overset{\text{def.}}{=} a\lambda^2$ is a new dimensionless measure of the amplitude. The transformation (6.9) thus treats a pair of solutions with the same dimensionless amplitude as a part of the same "family" of solutions. In these new coordinates it is impossible to perform the limit $\rho_{\max} \to 0^+$ for reasons mentioned above[2].

We are now going to calculate the proper distance from the "ring" to an arbitrary point $(\overline{\rho},\overline{z})$ in the meridional plane. The line segment is given by (3.6) in the new $(\tilde{\rho},\tilde{z},\phi)$ coordinates, and so the distance is given by

$$d = \left|\int_{\mathcal{L}} \mathrm{d}\iota\right| = \left|\int_0^{\frac{\overline{z}}{\sin\alpha}} \sqrt{g_{\rho\rho}(k\ \cos\alpha+\rho_{\max}, k\ \sin\alpha)}\sqrt{\left(\frac{\partial\rho}{\partial k}\right)^2+\left(\frac{\partial z}{\partial k}\right)^2}\ \mathrm{d}k\right| =$$
$$\left|\int_0^{\frac{\overline{z}}{\sin\alpha}} \exp\left[\frac{\Lambda(k\cos\alpha+\rho_{\max})^2}{1+(k^2+2k\rho_{\max}\cos\alpha+\rho_{\max}^2)^{\frac{n}{2}}}\right]\ \mathrm{d}k\right|. \tag{6.11}$$

Figure 6.5 shows several contour plots of the distance d to the "ring" in a given meridional plane for different values of the parameters $[\Lambda, n]$. We can see that the distance changes drastically for different values of the two parameters and the "ring" get strongly "directional", meaning that the proper distance strongly depends on the direction from where the ring is being approached.

Solutions with high Λ correspond to a family of solutions with high amplitude a (for a fixed wavelength λ). In this limit the seed function (6.1) approaches infinity pointwise everywhere besides the z-axis (where it always vanishes) and thus all spatial points (with the exclusion of the z-axis, of course) are infinitely remote. In a similar manner, for high negative amplitudes Λ the distance between any two points off the symmetry axis vanish.

The limit of high values of n (which affects asymptotic behavior of the seed function) will prove not physically interesting for our applications. In this limit the dimensionless form of the seed function (6.10) becomes

$$q(\rho,z) = \Lambda\frac{\rho^2}{1+(z^2+\rho^2)^{\frac{n}{2}}} \overset{n\to\infty}{\to} \begin{cases} 0, & \sqrt{\rho^2+z^2} > 1 \\ \Lambda\rho^2, & \sqrt{\rho^2+z^2} < 1 \end{cases}$$

[2]See the next Section for more details.

which is not a continuous function along the semicircle $\sqrt{\rho^2+z^2}=1$. Figure 6.4 shows the contour plot of the distance from the "ring" in the above $n\to\infty$ limit using Eq. (6.11). The discontinuity of the seed function as well as the flatness of the $\sqrt{\rho^2+z^2}>1$ region is not analogous to any of the ring sources. We will not explore this limit any closer. Let us just note that the proper radius

$$b=\int_0^{\rho_{\max}}\sqrt{g_{\rho\rho}(\rho,0)}\mathrm{d}\rho=\int_0^{\rho_{\max}}\exp\left[\Lambda\frac{\rho^2}{1+\rho^n}\right]\mathrm{d}\rho, \tag{6.12}$$

stays finite and takes the form

$$b=\int_0^1 e^{\Lambda\rho^2}\mathrm{d}\rho,$$

in the above limit.

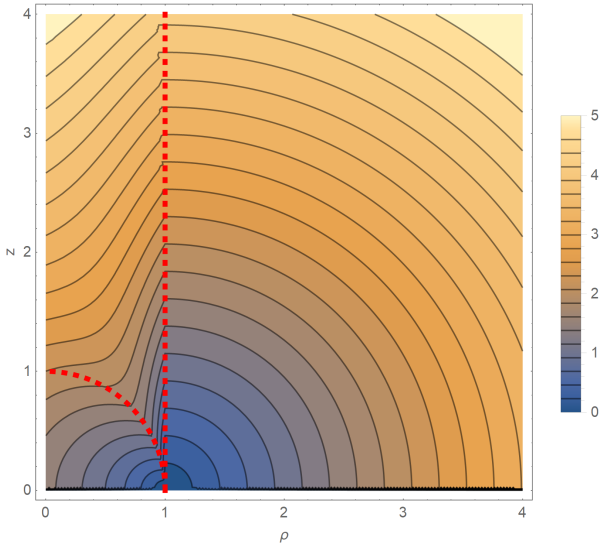

Figure 6.4: Contour plot of the distance d from the "ring" in the limit $n\to\infty$. The red line shows the condition $k+2\cos\alpha=0$.

6.4 Limit $\rho_{\max}\to 0^+$

At the beginning of this Chapter, we have shown that the radius of the "ring" is given by (6.2) and does not depend on the measure of the amplitude a. The limit $\rho_{\max}\to 0^+$ in this original form is then equivalent to $\lambda\to 0^+$ for $\forall n\in[4,\infty)$. Then, the seed function (6.1) is identically zero everywhere and we get flat Minkowski space

$$\mathrm{d}s^2=-\mathrm{d}t^2+\mathrm{d}\rho^2+\mathrm{d}z^2+\rho^2\mathrm{d}\phi^2. \tag{6.13}$$

In order to compute the proper distance from the "ring", we have converted the seed function to a dimensionless coordinates (6.10) using the transformation (6.9). In these coordinates, the ring position is only given by the parameter n

$$\tilde{\rho}_{\max}=\left(\frac{2}{n-2}\right)^{\frac{1}{n}}, \tag{6.14}$$

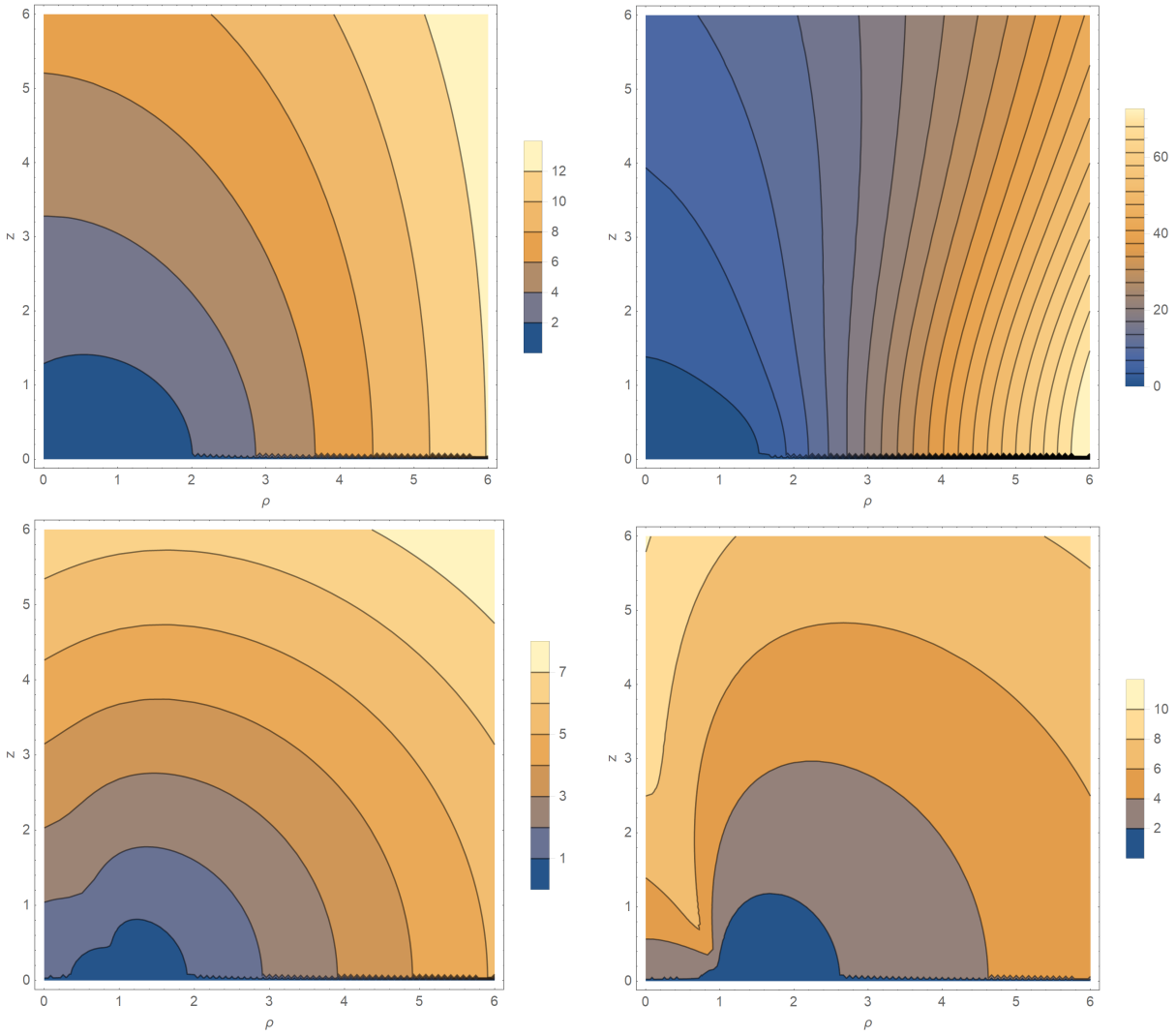

Figure 6.5: Contour plot of the distance d from the "ring" for different values of the constants $[\Lambda, n]$: Top left $[1, 4]$, top right $[3, 4]$, bottom left $[1, 100]$ and bottom right $[3, 1000]$.

which is a positive quantity that reaches its minimum at (see Figure 6.1)

$$n_{\min} \doteq 9.18 \implies \tilde{\rho}_{\max}(n_{\min}) \doteq 0.87,$$

and so the limit $\rho_{\max} \to 0^+$ is "inaccessible" for any fixed value of n. However, considering the definition of the dimensionless amplitude $\Lambda \overset{\text{def.}}{=} a\lambda^2$, for a fixed value of a the dimensionless amplitude Λ goes to zero and we get the flat Minkowski space point wise.

The "inaccessibility" of the $\rho_{\max} \to 0^+$ can be explained by the fact that the transformation (6.9) for $\lambda = 0$ is not a diffeomorphism as it maps the meridional plane to the origin and thus the inverse transformation does not exist. For $\forall \lambda > 0$ the "coordinate radius" $\tilde{\rho}_{\max} > 0$ is positive and so a simple continuous limit does not exist.

7. Geodesic motion

In this Chapter we will study simple cases of free motion of test particles in the static Brill space-time described by (5.4). As mentioned above, considering the solution static can only be justified for a short amount of time near the moment of time symmetry or in the presence of the source given by (5.14). We will assume that one of these conditions is met in the following.

7.1 Time of flight

In any meridional plane, there are only two absolute points between which the time of flight can be calculated. Those are the coordinate center, i.e. the intersection of the equatorial plane with the symmetry axis, and the "ring" itself. To calculate the time of flight we consider time-like motion in the ρ-direction. Normalization of the 4-velocity yields

$$-1 = g_{\mu\nu}u^\mu u^\nu = g_{tt}(u^t)^2 + g_{\rho\rho}(u^\rho)^2, \tag{7.1}$$

where $u^\rho = \frac{\mathrm{d}\rho}{\mathrm{d}\tau}$ and $\epsilon \overset{\text{def.}}{=} -g_{tt}u^t$ is the conserved energy per unit rest mass, invariantly given by

$$-\epsilon = g_{\mu\nu}\eta^\mu u^\nu = g_{tt}u^t = u_t = \frac{\mathrm{d}x_t}{\mathrm{d}\tau} = -\frac{\mathrm{d}t}{\mathrm{d}\tau}, \tag{7.2}$$

where we have used the fact that the metric is diagonal with $g_{tt} = -1$. This quantity is invariant and evaluating it in the asymptotic region where the space time becomes Minkowski yields

$$\frac{\mathrm{d}t}{\mathrm{d}\tau} = \frac{\mathrm{d}t}{\sqrt{-\eta_{\mu\nu}\mathrm{d}x^\mu \mathrm{d}x^\nu}} = \frac{1}{\sqrt{-\eta_{\mu\nu}\frac{\mathrm{d}x^\mu}{\mathrm{d}t}\frac{\mathrm{d}x^\nu}{\mathrm{d}t}}} = \frac{1}{\sqrt{1-\delta_{\mathrm{ij}}v^{\mathrm{i}}v^{\mathrm{j}}}} = \frac{1}{\sqrt{1-v^2}} \equiv \gamma. \tag{7.3}$$

Eq. (7.1) then becomes

$$\left(\frac{\mathrm{d}\rho}{\mathrm{d}\tau}\right)^2 = \frac{1}{g_{\rho\rho}}\left(\frac{\epsilon^2}{-g_{tt}} - 1\right) = \frac{\epsilon^2 - 1}{e^{2q(\rho,0)}}, \tag{7.4}$$

therefore

$$\frac{\mathrm{d}\tau}{\mathrm{d}\rho} = \frac{e^{q(\rho,0)}}{\sqrt{\epsilon^2-1}}. \tag{7.5}$$

The time of flight from $\rho = 0$ to $\rho = \rho_{\max}$ is given by

$$T = \int_0^T \mathrm{d}\tau = \int_0^{\rho_{\max}} \frac{\mathrm{d}\tau}{\mathrm{d}\rho}\,\mathrm{d}\rho = \frac{1}{\sqrt{\epsilon^2-1}}\int_0^{\rho_{\max}} e^{q(\rho,0)}\,\mathrm{d}\rho = \frac{b}{\sqrt{\epsilon^2-1}}, \tag{7.6}$$

where b is the proper radius of the ring given by (3.3) and (6.12), respectively. We can see that T is finite except in the case $\epsilon = 1$, i.e., $|\vec{p}| = 0$, corresponding to a particle which stays at the origin forever.

Photons moving radially in the "ring" plane follow null geodesics given by

$$0 = \mathrm{d}s^2 = g_{\mu\nu}\mathrm{d}x^\mu \mathrm{d}x^\nu = g_{tt}\mathrm{d}t^2 + g_{\rho\rho}\mathrm{d}\rho^2, \tag{7.7}$$

or

$$\rho_{,t} \equiv \frac{\mathrm{d}\rho}{\mathrm{d}t} = \pm e^{-q(\rho,0)}, \tag{7.8}$$

which is the local slope of the light cone for photons moving in the ρ-direction viewed by a stationary observer at the origin. Similarly, for photons moving parallel to the z-axis one gets

$$z_{,t} \equiv \frac{\mathrm{d}z}{\mathrm{d}t} = \pm e^{-q(0,z)}. \tag{7.9}$$

These two derivatives define the cone fully as we can see by performing the coordinate transformation

$$\begin{aligned} \rho &= \alpha\tilde{\rho} + \beta\tilde{z}, \\ z &= \beta\tilde{\rho} - \alpha\tilde{z}, \end{aligned} \tag{7.10}$$

with the condition $\alpha^2 + \beta^2 = 1$. Then the metric (1.1) becomes

$$\begin{aligned} \mathrm{d}l^2 = e^{2q(\rho,z)}[(\alpha\mathrm{d}\tilde{\rho} + \beta\mathrm{d}\tilde{z})^2 + (\beta\mathrm{d}\tilde{\rho} - \alpha\mathrm{d}\tilde{z})^2] + (\alpha\tilde{\rho} + \beta\tilde{z})^2\mathrm{d}\phi^2 \overset{\alpha^2+\beta^2=1}{=} \\ e^{2q(\rho,z)}(\mathrm{d}\tilde{\rho}^2 + \mathrm{d}\tilde{z}^2) + (\alpha\tilde{\rho} + \beta\tilde{z})^2\mathrm{d}\phi^2, \end{aligned} \tag{7.11}$$

and thus

$$\begin{aligned} \rho_{,t} &= \tilde{\rho}_{,t}, \\ z_{,t} &= \tilde{z}_{,t}. \end{aligned} \tag{7.12}$$

Figure 7.1 shows contour plot of the light-cone slope for photons moving in the meridional plane for $A = \pm 1$ and $\rho_0 = 0$. We can see that the cone gets "wider" at the peak of the wave for positive values of the amplitude parameter A and "narrower" for negative ones.

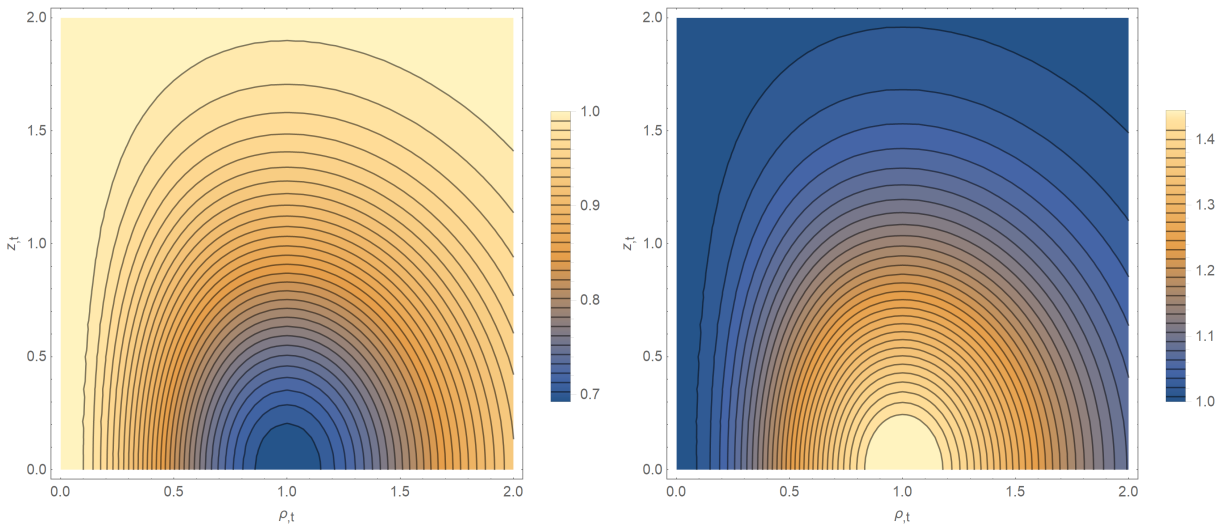

Figure 7.1: Contour plot of the light-cone slope in the meridional plane for $A = 1$ (left), $A = -1$ (right) and $\rho_0 = 0$ viewed by a stationary observer at the origin.

7.2 Gravitational acceleration

An important invariant affecting the motion of test particles in a given space-time is the gravitational acceleration. In the Newtonian limit one can show using the equation of geodesic motion that

$$g_{tt} \propto -1 - 2\Phi, \tag{7.13}$$

which can be thought of as first two terms in the expansion of $-e^{2\Phi} \stackrel{\text{def.}}{=} -N^2$. Here Φ denotes the Newtonian gravitational potential. To get the analogue of the gravitational acceleration, we consider the definition

$$\kappa_\mu \stackrel{\text{def.}}{=} -N_{,\mu} = -N\Phi_{,\mu}, \tag{7.14}$$

Using (7.13) we can evaluate the invariant square of the gravitational acceleration

$$\kappa^2 = g^{\mu\nu} N_{,\mu} N_{,\nu} = g^{\mu\nu} N^2 \Phi_{,\mu} \Phi_{,\nu}. \tag{7.15}$$

In our case, the gravitational acceleration vanishes as $g_{tt} = -N^2 = -1$. This is consistent with the fact that the mass-energy (5.22) is zero.

7.3 Circular geodesics

The potential existence and position of the photon orbit is the next invariant feature of the space-time which we will focus on. For a general Weyl space-time whose metric is given by (5.2) the photon circular orbit in the "ring" plane $z = 0$ is ([1], see Appendix C for a full proof)

$$2\rho A_{,\rho} = 1. \tag{7.16}$$

In our case $A = 0$ and thus there are no circular photon orbits.

We can also try to look for circular geodesics in the equatorial plane. One can see from reflection symmetry about the equatorial plane that the test particle with the initial velocity pointing in the equatorial plane will stay in that plane. From the 4-velocity normalization we get the condition

$$-1 = g^{\mu\nu} u_\mu u_\nu = g^{tt}(u_t)^2 + g^{\rho\rho}(u_\rho)^2 + g^{\phi\phi}(u_\phi)^2. \tag{7.17}$$

Using (1.1) and (7.37) we get

$$u_\rho = \pm e^{q(\rho,0)} \sqrt{\epsilon^2 - \left(1 + \frac{l^2}{\rho^2}\right)}. \tag{7.18}$$

In order for the motion to be circular, we require $u_\rho = 0$ and $u_{\rho,\rho} = 0$ at the radius of the circular orbit $\rho = \rho_c$. These conditions yield the pair of equations

$$\begin{aligned} 0 &= \epsilon^2 - 1 - \frac{l^2}{\rho_c^2}, \\ 0 &= \frac{l^2}{\rho_c^2 \sqrt{(\epsilon^2 - 1)\rho_c^2 - l^2}}, \end{aligned} \tag{7.19}$$

which only have one trivial solution $l = 0$ and $\epsilon = 1$, i.e. a static particle. This corresponds to the fact that the potential energy term $1 + \frac{l^2}{\rho^2}$ has no local maxima for nontrivial values of l.

If we consider motion of the test particles in the meridional plane, we can use the same symmetry argument (since the axial symmetry implies reflection symmetry about every meridional plane) as above to conclude that the motion will be confined to that plane. The normalization condition for 4-velocity now reads

$$-1 = g^{\mu\nu}u_\mu u_\nu = g^{tt}(u_t)^2 + g^{\rho\rho}(u_\rho)^2 + g^{zz}(u_z)^2, \tag{7.20}$$

or (using the fact $g_{zz} = g_{\rho\rho}$ and (5.4))

$$(u_\rho)^2 + (u_z)^2 = g_{\rho\rho}(\epsilon^2 - 1) = (\epsilon^2 - 1)e^{2q(\rho,z)}. \tag{7.21}$$

Let us refer to Eq. (7.36) in advance. Using the first form of the seed function (1.4) we get

$$\begin{aligned} \frac{\mathrm{d}u_z}{\mathrm{d}\tau} &= -2A\rho^2 z \exp\left(2A\rho^2 e^{-(\rho-\rho_0)^2-z^2} - (\rho-\rho_0)^2 - z^2\right)[(u^\rho)^2 + (u^z)^2], \\ \frac{\mathrm{d}u_\rho}{\mathrm{d}\tau} &= -2A\rho\left(\rho^2 - \rho\rho_0 - 1\right)\exp\left[2A\rho^2 e^{-(\rho-\rho_0)^2-z^2} - (\rho-\rho_0)^2 - z^2\right][(u^\rho)^2 + (u^z)^2]. \end{aligned} \tag{7.22}$$

We can see there is one equilibrium point at the origin which is in agreement with the calculation above. Figure 7.2 shows a contour plot of the prefactor $g_{zz,\rho}$ in the second equation for $A = 1$ and $\rho_0 = 0$. We note that the acceleration is zero in the ρ-direction at the "ring", i.e. where $\rho = \rho_{\max}$. This is interesting since the square of total 3-velocity does not change the sign of the acceleration. For positive amplitudes the test particles are accelerated towards the ρ-axis in the z-direction. A closed orbit around the origin is not possible as for $A > 0$ the particles are accelerated towards the "ring" in the ρ-direction and for $A < 0$ the acceleration in the z-direction points away from the ρ-axis.

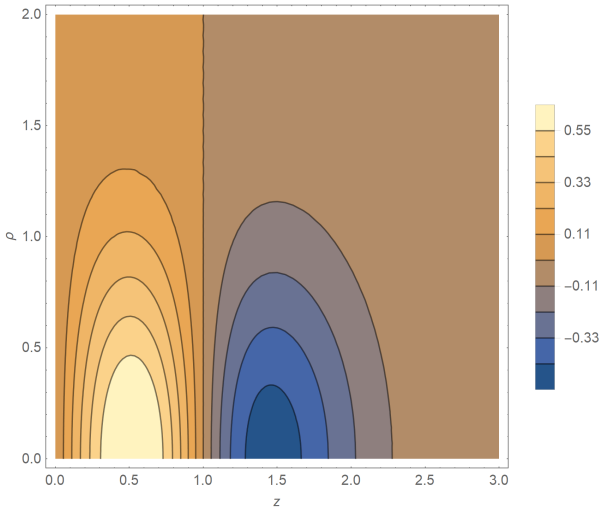

Figure 7.2: The derivative of the covariant metric $g_{zz,\rho}$ for $A = 1$ and $\rho_0 = 0$ determining the sign of the acceleration in the ρ-direction.

There may exist closed orbits around the "ring" itself, however, we will not focus on them here. Let us just note that this is possible only for $A > 0$ since for $A < 0$ the test particles are accelerated "away" from the "ring" in both directions.

Conclusion

We have presented a way to treat the Brill space-time around the moment of time symmetry as a static approximation of a "ring"-like source. We have seen in Chapters 3 and 6 that both choices of the seed functions (1.1) and (6.1) yield satisfactory geometrical properties of the "ring". Both exhibit finite small and large circumferences and their proper radius is also finite. This static solution is intended as an approximation of the material thin-ring sources and thus these simple properties are satisfactory.

We have also seen that the proper radius (3.3) and (6.6) is not a monotonically increasing function of their "coordinate radius" defining variables ρ_0 and λ, respectively, for negative values of the amplitude parameters A and a. We have also seen in Subsection 5.1.1 that the equatorial plane is not asymptotically flat for negative values of A. However, the extreme of the 3D Ricci tensor for negative A follows the "coordinate radius" $\rho_{\max}$ closer for high values of ρ_0 (see Figure 5.3) where the proper radius is monotonically incresing with λ (see Figure 3.2).

In Chapter 5, we have shown that the full 4-metric of the static Brill space-time is given by (5.4) and we calculated its energy-momentum tensor using the Einstein equations. As expected, the source turned out not to be "physically meaningful" as its invariant Killing components $T_{tt} = T_{\phi\phi}$ indicate the existence of areas with positive and negative energy density which violates the weak energy condition

$$T_{\mu\nu}u^{\mu}u^{\nu} \geq 0,$$

for any time-like u^{μ}. Using the Tolman integral (5.22), we have found that the total mass of the space-time vanishes.

In Chapter 7 we showed that there are no circular photon or particle orbits in the equatorial plane. This is in contrast with the thin rings [1]. This shows that the static Brill space-time is not a suitable approximation if one wishes to study the motion of particles.

Appendix A

The nonzero Christoffel symbols given by (4.4) are

$$\begin{aligned}
\overline{\Gamma}^{\rho}{}_{\rho\rho} &= \partial_\rho q(\rho,z),\\
\overline{\Gamma}^{\rho}{}_{\rho z} &= \partial_z q(\rho,z),\\
\overline{\Gamma}^{\rho}{}_{z\rho} &= \partial_z q(\rho,z),\\
\overline{\Gamma}^{\rho}{}_{zz} &= -\partial_\rho q(\rho,z),\\
\overline{\Gamma}^{\rho}{}_{\phi\phi} &= \rho e^{-2q(\rho,z)},\\
\overline{\Gamma}^{z}{}_{\rho\rho} &= -\partial_z q(\rho,z),\\
\overline{\Gamma}^{z}{}_{\rho z} &= \partial_\rho q(\rho,z),\\
\overline{\Gamma}^{z}{}_{z\rho} &= \partial_\rho q(\rho,z),\\
\overline{\Gamma}^{z}{}_{zz} &= \partial_z q(\rho,z),\\
\overline{\Gamma}^{\phi}{}_{\rho\phi} &= \frac{1}{\rho},\\
\overline{\Gamma}^{\phi}{}_{\phi\rho} &= \frac{1}{\rho},
\end{aligned} \tag{7.23}$$

where for the first choice of the seed function q given by (1.2) we have

$$\begin{aligned}
\partial_\rho q(\rho,z) &= -2A\rho(\rho^2-\rho\rho_0-1)e^{-(\rho_0-\rho)^2-z^2},\\
\partial_z q(\rho,z) &= -2A\rho^2 z e^{-(\rho_0-\rho)^2-z^2}.
\end{aligned} \tag{7.24}$$

For the second form given by (6.1) we have

$$\begin{aligned}
\partial_\rho q(\rho,z) &= \frac{a\rho\left(2\lambda^{-n}\left(\rho^2+z^2\right)^{n/2}-n\rho^2\lambda^{-n}\left(\rho^2+z^2\right)^{\frac{n}{2}-1}+2\right)}{\left(\lambda^{-n}\left(\rho^2+z^2\right)^{n/2}+1\right)^2},\\
\partial_z q(\rho,z) &= -\frac{an\rho^2 z\lambda^n\left(\rho^2+z^2\right)^{\frac{n}{2}-1}}{\left(\lambda^n+\left(\rho^2+z^2\right)^{n/2}\right)^2}.
\end{aligned} \tag{7.25}$$

The Ricci tensor in the (ρ,z,ϕ) base is

$$\overline{R}_{ji}=\begin{pmatrix}
\frac{1}{\rho}q_{,\rho}(\rho,z)-q_{,zz}(\rho,z)-q_{,\rho\rho}(\rho,z) & \frac{1}{\rho}q_{,z}(\rho,z) & 0\\
\frac{1}{\rho}q_{,z}(z\rho,z) & -\frac{1}{\rho}q_{,\rho}(\rho,z)-q_{,zz}(\rho,z)-q_{,\rho\rho}(\rho,z) & 0\\
0 & 0 & 0
\end{pmatrix}. \tag{7.26}$$

For the seed function given by (1.2) we have

$$\begin{aligned}
\overline{R}_{11} &= 2A\left(-\rho^2+\rho\rho_0+1\right)e^{-(\rho_0-\rho)^2-z^2}\\
&\quad -2Ae^{-(\rho_0-\rho)^2-z^2}\left(2\rho^4+2\rho^2\rho_0^2-4\left(\rho^2-1\right)\rho\rho_0+2\rho^2\left(z^2-3\right)+1\right),\\
\overline{R}_{12} &= R_{21} = -2A\rho z e^{-(\rho_0-\rho)^2-z^2},\\
\overline{R}_{22} &= 2A\left(\rho^2-\rho\rho_0-1\right)e^{-(\rho_0-\rho)^2-z^2}\\
&\quad -2Ae^{-(\rho_0-\rho)^2-z^2}\left(2\rho^4+2\rho^2\rho_0^2-4\left(\rho^2-1\right)\rho\rho_0+2\rho^2\left(z^2-3\right)+1\right).
\end{aligned} \tag{7.27}$$

Appendix B

To show that the total Tolman mass m vanishes in the special case of the seed function given by (6.1), we consider the asymptotic solution of the Hamiltonian constraint (4.2). Using the simplified version of the transformed seed function (6.10) and the general expression for the Ricci scalar (4.7), we have (we omit tilde in the following)

$$
\begin{aligned}
{}^3\overline{R} = -2e^{-2q(\rho,z)} & \frac{\Lambda(\rho^2(n^2((\rho^2+z^2)^n-(\rho^2+z^2)^{n/2})+n(-4(\rho^2+z^2)^{n/2}-4(\rho^2+z^2)^n)}{(\rho^2+z^2)((\rho^2+z^2)^{n/2}+1)^3} \\
& + 2e^{-2q(\rho,z)} \frac{+2((\rho^2+z^2)^{n/2}+1)^2)+2z^2((\rho^2+z^2)^{n/2}+1)^2)}{(\rho^2+z^2)((\rho^2+z^2)^{n/2}+1)^3}. \quad (7.28)
\end{aligned}
$$

Along the x-axis, the Hamiltonian constrain (4.2) takes the form

$$
\frac{\partial^2\psi}{\partial x^2} + \frac{\Lambda}{4}\frac{n^2(x^{2n}-x^n)-3n(x^n+x^{2n})+2(x^n+1)^2}{(x^n+1)^3} e^{\frac{2ax^2}{x^n+1}}\psi = 0. \quad (7.29)
$$

In the limit $x \to \infty$, Eq. (7.29) becomes

$$
\frac{\partial^2\psi}{\partial x^2} = 0,
$$

with solution

$$
\psi(x) = c_0 + c_1 x. \quad (7.30)
$$

We then consider the asymptotic solution of (7.29) in the form

$$
\psi(x) = (c_0 + c_1 x)(1 + \psi_1(x) + \psi_2(x) + \dots), \quad (7.31)
$$

where $\psi_i(x)$ are unknown functions of x. We also assume $\psi_i(x) \gg \psi_{i+1}(x)$, $\forall i \in \mathbb{N}$ as $x \to \infty$ along with all its derivatives since we expect $\psi_i(x) \sim x^{-i}$.

In (1.6), we assume that the conformal factor decays as in the Schwarzschild metric. Therefore, to obtain an expression for the total mass-energy of the wave, one needs to evaluate the constant at the $\sim r^{-1}$ term of the asymptotic expansion of ψ.

We want the solution to be asymptotically flat, so we choose

$$
\begin{aligned}
c_0 &= 1, \\
c_1 &= 0,
\end{aligned} \quad (7.32)
$$

and look for the solution in the form

$$
\psi(x) = 1 + \psi_1(x) + \psi_2(x) + \dots. \quad (7.33)
$$

Asymptotic expansion at infinity yields

$$
\frac{n^2(x^{2n}-x^n)-3n(x^n+x^{2n})+2(x^n+1)^2}{(x^n+1)^3} \sim \frac{1}{x^n} + o\left(\frac{1}{x^{n+1}}\right),
$$

and thus to the first order in ψ_i we get from (7.29), for $n = 4$,

$$\frac{\partial^2 \psi_1}{\partial x^2} + \frac{\Lambda}{4}\left(\frac{8}{x^4} + o\left(\frac{1}{x^5}\right)\right) e^{\dfrac{2ax^2}{x^4+1}}(1+\psi_1) = 0. \tag{7.34}$$

Let us multiply the equation by x^4 and perform the limit $x \to \infty$:

$$\lim_{x\to\infty} x^4 \frac{\partial^2 \psi_1}{\partial x^2} = -2\Lambda = \text{const.} \iff \lim_{x\to\infty} \psi_1 = 0.$$

Integrating twice and setting the integration constants to zero (to satisfy the above $x \to \infty$ behaviour) yields

$$\frac{\partial^2 \psi_1}{\partial x^2} = -2\frac{\Lambda}{x^4} \implies \psi_1(x) = -\frac{\Lambda}{6x^2},$$

and so the first term decays as x^{-2} which implies $m = 0$.

Alternatively, one can use Eq. (1.5) along x-axis with asymptotic behavior of ψ given by (1.6), to obtain

$$m = \lim_{x\to\infty} x^3 \psi''(x) = \lim_{x\to\infty} \frac{x^3}{4}\left(\frac{q_{,x}}{x} - q_{,xx}\right)\psi(x) = 0.$$

Appendix C

We consider the geodesic equation with the 4-velocity $\frac{\mathrm{d}x^\mu}{\mathrm{d}\tau} = u^\mu$,

$$\frac{\mathrm{d}u_\alpha}{\mathrm{d}\tau} - \Gamma_{\sigma\alpha\beta}u^\sigma u^\beta = 0. \tag{7.35}$$

Using Eq. (4.4) we get

$$\frac{\mathrm{d}u_\alpha}{\mathrm{d}\tau} = \frac{1}{2}(g_{\sigma\alpha,\beta} + g_{\beta\sigma,\alpha} - g_{\alpha\beta,\sigma})u^\sigma u^\beta = \frac{1}{2}g_{\beta\sigma,\alpha}u^\sigma u^\beta, \tag{7.36}$$

where we have used the symmetry of the metric $g_{\mu\nu} = g_{\nu\mu}$ and antisymmetry of the term $g_{\sigma\alpha,\beta} - g_{\alpha\beta,\sigma}$ in σ-β.

We consider static and axially symmetric solution, so (7.36) yields two integrals of motion,

$$\begin{aligned} u_t &= \text{const.} \overset{(7.2)}{=} -\epsilon, \\ u_\phi &= \text{const.} \end{aligned} \tag{7.37}$$

As mentioned above, ϵ is the conserved energy per rest mass. Similarly, $u_\phi = g_{\phi\phi}\frac{\mathrm{d}\phi}{\mathrm{d}t}\frac{\mathrm{d}t}{\mathrm{d}\tau} \equiv l$ is the angular momentum with respect to an observer at spatial infinity per rest mass.

To derive the equation for photon orbit in Weyl space-time whose metric is given by (5.2), we use normalization of 4-momentum for photons moving in the "ring" plane,

$$0 = g^{\mu\nu}p_\mu p_\nu = g^{tt}(p_t)^2 + g^{\phi\phi}(p_\phi)^2 + g^{\rho\rho}(p_\rho)^2, \tag{7.38}$$

from where, using (7.37), we get

$$(p_\rho)^2 = g_{\rho\rho}(-g^{tt}E^2 - g^{\phi\phi}L^2) \overset{(5.2)}{=} e^{2(B-A)}(-e^{-2A}E^2 - \frac{1}{\rho^2}e^{2A}L^2) = -e^{2B-4A}E^2 - \frac{e^{2B}}{\rho^2}L^2. \tag{7.39}$$

In order for the trajectory to be circular, the radial momentum must vanish together with its derivative $p_\rho = 0$ and $p_{\rho,\rho} = 0$ (this latter condition corresponds to the photon being at the local extreme of the potential term $\frac{e^{2B}}{\rho^2}L^2$). Thanks to the first condition we can work with $(p_\rho)^2_{,\rho} = 0$. We obtain the pair of equations

$$\begin{aligned} 0 = &-e^{2B-4A}E^2 - \frac{e^{2B}}{\rho^2}L^2, \\ 0 = &-2(B-2A)_{,\rho}e^{2B-4A}E^2 - 2(\rho B_{,\rho} - 1)\frac{e^{2B}}{\rho^3}L^2. \end{aligned} \tag{7.40}$$

Solving for A yields

$$1 = 2\rho A_{,\rho}. \tag{7.41}$$

Bibliography

[1] Oldřich Semerák, *Static axisymmetric rings in general relativity: How diverse they are*, Physical Review D 94, (2016), 104021

[2] Brill D. R., *On the Positive Definite Mass of the Bondi-Weber-Wheeler Time-Symmetric Gravitational Waves*, Annals of Physics, 7, 466-483, (1959)

[3] hirnov A., Ledvinka T., *Gauge Choice in Numerical Evolution of the Brill Data*, (2015)

[4] de Oliveira H. P., Rodrigues E. L., *Brill wave initial data: Using the Galerkin-collocation method*, Physical Review D 86, (2012), 064007

[5] Weyl H., *Zur Gravitationstheorie*, Annalen der Physik 54, 117–145, (1917) English Translation: Weyl H., *Republication of: 3. On the theory of gravitation*, General Relativity and Gravitation 44: 779-810, (2012)

[6] Garfinkle D., Duncan G. C., *Numerical evolution of Brill waves*, arXiv:gr-qc/0006073, (2000)

[7] Florides P. S., *On the Tolman and Møller mass-energy formulae in general relativity*, Journal of Physics: Conference Series 189, (2009), 012014

List of Figures

List of Tables